Master's thesis

NTNU
Norwegian University of Science and Technology
Faculty of Engineering
Department of Marine Technology

Martin Guneriussen

Analysis of the Havfarm concept for extreme envoirnmental loads

Master's thesis in Marine Technology
Supervisor: Jørgen Amdahl
Co-supervisor: Martin Slagstad
June 2022

NTNU
Norwegian University of
Science and Technology

Martin Guneriussen

Analysis of the Havfarm concept for extreme envoirnmental loads

Master's thesis in Marine Technology
Supervisor: Jørgen Amdahl
Co-supervisor: Martin Slagstad
June 2022

Norwegian University of Science and Technology
Faculty of Engineering
Department of Marine Technology

NTNU
Norwegian University of
Science and Technology

NTNU
Kunnskap for en bedre verden

Department of Marine Technology

Martin Guneriussen

Analysis of the Havfarm concept for extreme environmental loads

Supervisor: Jørgen Amdahl
Co-Supervisor: Martin Slagstad

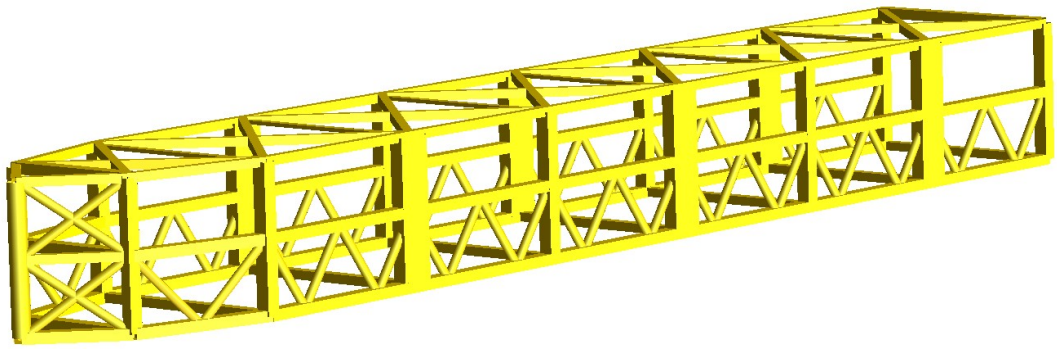

10th June 2022

Preface

This Master thesis is the synopsis of a 5 years study at the Institute for Marine Technology(IMT). The intended reader is one with knowlegde of the field, and some understanding of both hydrodynamic and structural processes.

I want to take this opportunity to thank my supervisor Prof. Jørgen Amdahl, enabling me to build a basis understanding of the themes, being a sparring partner and providing general guidance while i wrote this thesis. Further, thanks is due to my co-supervisor Martin Slagstad for method suggestions, resources to look into and assistance with executable necessary for post processing. In addition to the supervisors on this project, there has been a great deal of help in reading the master theses written by MSc Holen and MSc Gulpinar in which the studied model is established, design choices motivated and analysis of said model performed.

I have both thoroughly enjoyed my stay, and had uphill battles due to the rigorous academic standards introduced to me. It has been a pleasantly challenging road to travel. I look forward to starting a new chapter in my life, while simultaneously regret that I am leaving.

IMT is due to get torn to pieces, and rebuilt. Similar to what studying Marine Technology has helped me do.

Trondheim, June 10th 2022

Martin Guneriussen

Abstract

Motivated by the desire to move to more exposed waters to retain their growth, the aquaculture industry has developed innovative designs in the last couple of years. Fueled by an increase in food demand and backed by the Norwegian government and third-party actors through development licenses and updates on their regulations and practices. One such innovative structure is Nordlaks' Havfarm 1, examined in this master thesis.

The torsional eigenmode of the structure is a reoccurring theme and is examined thoroughly by different methods. A simplified model created during earlier written master theses' has been modified and utilized for this purpose. Initial calculations and simple simulations confirm earlier estimations of RBMs and further find the torsional and bending eigenperiod to be 4 and 1.5 seconds respectively.

Transfer functions describing hull torsion and bending are established, confirming the eigenperiods found, a finding supporting the usage of linear methods.

An estimation based on an industry-developed contour line combined with stochastic simulations was used to confirm the applicability of the contour line method, here resulting in a $1.84874 * 10^{-2}[rad]$ relative roll, aft to bow.

The computational demand skyrockets when the simplified model includes the fish net. Thus a small sample of simulations became the basis for a slightly shifted transfer function. Having lower response amplitudes due to increased damping and a lower period for its resonance peak due to increased stiffness from the net implementation.

Multiple design wave methods were evaluated, with quite a variety of results. Based on the eigenperiod combined with wave steepness limit, the simplified design wave resulted in a $2.106 * 10^{-2}[rad]$ relative roll, aft to bow. A result that conforms with the result from stochastic simulations during the contour line method.

Sammendrag (Norsk)

Motivert av ønsket om å flytte til mer utsatte farvann for å fortsette veksten, har havbruksnæringen utviklet innovative design de siste par årene. Drevet av økt etterspørsel etter mat og støttet av norske myndigheter og tredjepartsaktører gjennom utviklingslisenser og oppdateringer av deres regelverk og praksis. En slik innovativ struktur er Nordlaks' Havfarm 1, undersøkt i denne masteroppgaven.

Den torsjonelle egenmodusen til strukturen er et tilbakevendende tema og undersøkes grundig med forskjellige metoder. En forenklet modell laget under tidligere skriftlige masteroppgaver har blitt modifisert og brukt til dette formålet. Innledende beregninger og enkle simuleringer bekrefter tidligere estimater av RBMer og finner videre at torsjons- og bøyningsegenperioden er henholdsvis 4 og 1,5 sekunder.

Transferfunksjoner som beskriver skrogtorsjon og bøyning er etablert, og bekrefter videre egenperiodene funnet, noe som støtter opp under bruken av lineære metoder.

Et estimat basert på en industriutviklet konturlinje kombinert med stokastiske simuleringer ble brukt for å bekrefte anvendeligheten av konturlinjemetoden, noe som her resulterte i en relativ rulling på $1,84874 * 10^{-2}[rad]$, akter til baug.

Beregningsbehovet skyter i været når den forenklede modellen inkluderer fiskenettet. Dermed ble et lite utvalg av simuleringer grunnlaget for en noe forskjøvet tranferfunksjon for torsjon. Den har lavere responsamplituder på grunn av økt demping og en lavere periode for resonanstoppen på grunn av økt stivhet fra nettimplementeringen.

Flere designbølgemetoder ble evaluert, med ganske varierende resultater. Basert på egenperioden kombinert med bølgebratthetsgrensen, resulterte den forenklede designbølgen i en relativ rulling på $2,106 * 10^{-2}[rad]$, akter til bue. Et resultat som samsvarer med resultatet fra stokastiske simuleringer under konturlinjemetoden.

Table of Contents

List of Figures

List of Tables

Nomenclature

Symbols

$\overline{GM}_T$	=	Transverse Metacentric height
$\overline{GM}_L$	=	Longitudinal Metacentric height
∇	=	Volume displacement of structure
ω	=	Angular wave frequency
ω_p	=	Angular spectral peak frequency
ρ	=	Water density
Re	=	Real part of complex number
β	=	Wave direction
C_M	=	Mass coefficient, morison
C_D	=	Drag coefficient, morison
ϕ_i	=	Response phase
D	=	Diameter
u	=	Horizontal water particle velocity
$\dot{u}$	=	Horizontal water particle acceleration
H_s	=	Significant wave height
T_p	=	Peak wave period
K_{wp}	=	Stiffness of water plane
T_z	=	Zero-uprcossing period
ξ_a	=	Wave amplitude

Abbreviations

RP	=	DNV Recommended Practice document
FE	=	Finite Element
ULS	=	Ultimate Limit State
FLS	=	Fatigue Limit State
RU	=	DNV Rules document
OU	=	DNV Offshore Units document
RAO	=	Response Amplitude Operator
RBM	=	Rigid Body Mode
FEM	=	Finite Element Model/Method
DNV	=	Det Norske Veritas
NORSOK	=	Norsk Sokkels Konkurranseposisjon
CMA	=	Conditional Modelling Approach
POV	=	Position of View
DOF	=	Degree of freedom
WSD	=	Working stress design
LRFD	=	load and resistance factor design

Thesis Outline

This Master thesis is based on the foundation laid throughout the autumn semester of 2021 and the resulting Project Thesis. The project mapped the theoretical environment in which this Master thesis will be constructed. The project thesis emphasis was laid on literature review, especially concerning the different standards available for being compliant with rules and regulations surrounding aquaculture.

For increased readability the report is assembled in a manner closely mimicking the included task description defining the scope.

NTNU
Norges teknisk-naturvitenskapelige universitet
Institutt for marin teknikk

Master thesis 2022

for

Stud. Techn. Martin Elling Guneriussen

Analysis of the Havfarm concept for extreme environmental loads

Analyse av Havfarm konseptet utsatt for ekstreme miljølaster

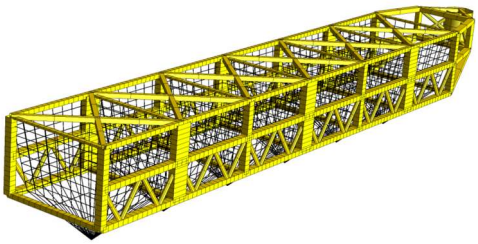

Marine fish farming is in rapid development. Dimensions are increasing and locations are being moved to areas exposed to more energetic waves and stronger currents. This leads to several challenges: Strong currents can cause large net deformations and affect largely the hydroelastic behaviour of the cage. Wave overtopping may occur in during extreme waves, so nonlinear effects matter. Viscous effects are essential for the loading on the net structures, as well as the wake inside the cage. Another issue is the effect of biofouling on the net loading. Waves and currents are of concern for the volume within the fish cage and the design of mooring lines.

Failure of fish farms, with large-scale fish escape to the level experienced in the past, will not be tolerated by the society. New and extreme loading scenarios need to be properly designed for by means of "*first principles"* methods to meet required safety levels and performance.

Rational design methods have been applied the design of Salmar's Ocean Farm 1 and Nordlaks' Havfarm1. The design is to a large degree based on principles and experience gained in the offshore oil and gas industry as regards fatigue and ultimate strength assessment. Although the structural performance is governed by effects that are similar to those for floating offshore structures, notable differences exist, e.g. the large size compared to predominant wave lengths, very location dependent wave and current conditions, current is generally more important , sloshing loads in closed or semi-closed compartments, and loads from the fish net.

The Havfarm1 fish farm concept has recently been installed outside the island Hadsel in Vesterålen, with a design sea state of H_s = 6 m. Plans are now being made to move fish farming into even more hostile waters. An important issue is to balance the demand for relatively calm wave conditions inside the farm to create a sustainable environment for the fish stock with requirements to strengthening of the structural members of the fish farm

The intention of this work is to get further insight into the loads and load effects of Havfarm1 type fish farm structures and to assess the structural response and performance of such concepts in increasingly exposed waters.

The work in the project is proposed carried out in the following steps:

1) A brief review of current rules and regulations for design of fish farms including NS 9415, offshore rules and relevant ship rules that may be applied.

2) Modify the existing model so that the "bow" section resembles more the real Havfarm1. Perform a critical review of mass distributions and added masses assumed. Check that model floats approximately on even keel in flat sea. Conduct eigenvalue analysis of the rigid body motions as well as bending and torsional motions of the fish farm. Compare with simple hand calculations to the extent possible.

3) Simulate the response of the fish farm in various regular waves (head waves and oblique waves) using scripting methods. Establish transfer functions for selected variables for the "linear" response (small waves) and the response for realistic wave amplitudes. Conclude whether the response can essentially be determined with linear methods.

4) Analyse the global response in irregular seas. Estimate the characteristic extreme response levels for selec ted response variables by means of the contour line method and repeated stochastic simulations. Compare with results from stochastic linear analysis

5) If time permits, conduct simulations of the fish farm with the net included. This will probably be very CPU-demanding, and the no. of simulations will be small. Comapre with the results obtained without the fish net.

6) Evaluate whether design wave methods may be used to estimate the maximum response in the fish farm.

7) Conclusions and recommendations for further work.

Literature studies of specific topics relevant to the thesis work may be included.

The work scope may prove to be larger than initially anticipated. Subject to approval from the supervisors, topics may be deleted from the list above or reduced in extent.

In the thesis the candidate shall present his personal contribution to the resolution of problems within the scope of the thesis work.

Theories and conclusions should be based on mathematical derivations and/or logic reasoning identifying the various steps in the deduction.

The candidate should utilise the existing possibilities for obtaining relevant literature.

Thesis format

The thesis should be organised in a rational manner to give a clear exposition of results, assessments, and conclusions. The text should be brief and to the point, with a clear language. Telegraphic language should be avoided.

The thesis shall contain the following elements: A text defining the scope, preface, list of contents, summary, main body of thesis, conclusions with recommendations for further work, list of symbols and acronyms, references and (optional) appendices. All figures, tables and equations shall be numerated.

The supervisors may require that the candidate, in an early stage of the work, presents a written plan for the completion of the work. The plan should include a budget for the use of computer and laboratory resources which will be charged to the department. Overruns shall be reported to the supervisors.

The original contribution of the candidate and material taken from other sources shall be clearly defined. Work from other sources shall be properly referenced using an acknowledged referencing system.

The report shall be submitted in two copies:

- Signed by the candidate
- The text defining the scope included
- In bound volume(s)
- Drawings and/or computer prints which cannot be bound should be organised in a separate folder.
- The report shall also be submitted in pdf format along with essential input files for computer analysis, spreadsheets, MATLAB files etc in digital format.

Ownership
NTNU has according to the present rules the ownership of the thesis. Any use of the thesis has to be approved by NTNU (or external partner when this applies). The department has the right to use the thesis as if the work was carried out by a NTNU employee, if nothing else has been agreed in advance.

Thesis supervisor
Prof. Jørgen Amdahl
PhD Martin Slagstad

Deadline: June 11, 2022
Trondheim, January 10, 2022

Jørgen Amdahl

Concept Background & Motivation

In 2019 the UN reported a 95% prediction interval from 9.8-12.8 billion, based on the Bayesian Hierarchical Model, for the World population in 2100. Leading to more mouths to feed, necessarily with a more sustainable approach than today's food production. It is in this relation that aquaculture fits in. Norway has reached a level of aquaculture activity considered saturated for sustainable production. Thus new solutions are necessary for continuing the growth of the industry.[34]

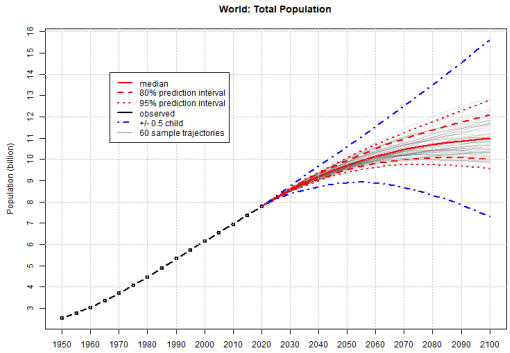

Figure 1: Population estimates made by the UN in 2019 [34]

The main challenges for the aquaculture industry are waste production, an increase in lice, salmon escaping, and production area shortage along the coast. The Norwegian Government wished to incite innovation within the aquaculture industry based on these challenges. As such, a program started giving developers the option to apply for development licenses. These licenses were appropriated with no cost, but came with the conditions that the concept was innovative, required substantial investments, and aimed to tackle the industry challenges. Applications were received for two years starting in November 2015, and some have yet been finalized. [10].

With all these elements and a practical design put forward, Nordlaks received several licenses. With these licenses, Nordlaks rolled out phase 1, being a turret moored structure partly enclosed by the coastline of Vesterålen in Northern Norway.

Nordlaks, and NSK Ship Design aim to use these licenses to research the possibilities of moving aquaculture toward offshore conditions and dimensions through Havfarm 1. Doing so would allow them to utilize the harsher and more exposed part of the Norwegian coastline and give the industry access to more surface area. Further benefits include distributing biological waste over a greater area and decreasing the strain put on the ecosystem. In addition, the more considerable distances between farms will help tremendously reduce the chance of lice infecting the farms.

There are several similarities between the model utilized throughout this thesis and the actual structure owned by Nordlaks. However, it is necessary to point out that this thesis is not based on a collaboration with either NSK Shipdesign or Nordlaks. Neither should the results be considered recommendations or criticism regarding the actual design, calculation, production, or operation of Havfarm 1, also known as *Jostein Albert*.

1 Literature review

A brief literature review regarding previous master projects, the applicability of load calculation methodology in utilized software, and relevant rules are presented in this section.

1.1 Previous Master theses

The foundation for this project thesis is the master theses of Vegard Holen and Jørgen Gulpinar, whom both have evaluated the Havfarm concept. Holen is the model's creator, further analyzed by Gulpinar, and will be further reviewed and adjusted as part of this thesis' scope.

1.1.1 Vegard Holen - Ultimate Limit State Analysis of Havfarm

The scope of Holens' Master thesis was to establish a finite element (FE) model of the fish farm in USFOS, including mooring lines and nets. Further, he was to perform an Ultimate Limit State (ULS) analysis of the Havfarm concept based on the established FEM model. The analysis investigated the concept of ULS performance in accordance with applicable rules and regulations. When Holen delivered his thesis, there were close to no resources describing the environmental conditions of the relevant area. This led to the use of guesstimates regarding what sea states to investigate.[16]

Holen encountered several problems regarding a stable numerical analysis. One was the net's stiffness contribution, implemented through the Modified Morison Model. The attempted modeling was cut short for the mooring, and a spring with a counteracting buoyancy element was introduced to represent the mooring. Holen later scrutinizes this modeling choice as it introduced a large degree of cyclical pitch-motion when evaluating the heave decay response.[16][27]

Holens' thesis shows that the structural model can support itself and passes the ULS design condition analysis performed. Holen comments that the yield utilization factor is substantially lower than expected, pointing to design choices as possible sources of error. One is the choice of implementing mass directly through the equivalent thickness of elements, with the thickness constant over elements and into the joints. Holen characterizes this as an unrealistic design that produces larger cross-sectional areas in the joints than could be considered realistic. He argues that since Fatigue Limit State (FLS) analysis is outside the scope of his thesis, this is not a huge concern. [16]

For the analysis, holen carried out 60 3-hour irregular stochastic simulations. He established a 90%-fractile utilization factor from these simulations by fitting the results to a Gumbel probability paper. The findings are that the structure model is in good compliance with investigated ULS criteria. Holen stated that the modeling was challenging, especially concerning the certainty of the results. Several model choices were made out of a lack of resources, time, and the lack of knowledge of the choices' effects. [16]

1.1.2 Jørgen Gulpinar - Analysis of the Havfarm concept for extreme environmental loads

"*At the time of writing, the fish farm has been built, towed to Norway, and is at the beginning of its production. The model Holen developed has been used as a basis for investigations into the USFOS program and behavior of Havfarm 1.*" (Gulpinar, 2021)[14]

Gulpinars' thesis describes and discusses modeling choices for the USFOS model established by Vegard Holen in the previously discussed Master thesis. This model, alongside the progress made on the project, is the framework for the renewed analysis of the Havfrarm concept. He found that the rules presented by the classification society DNV GL rebranded to DNV are the most applicable and up to date. A brief overview of the limit state design assessment is presented. The ULS assessment focuses on the Heave motion, as the yield utilization is found sufficient in Holens' master thesis. [14]

Methods of ULS analysis were presented, with the contour line method prevailing in the estimation of the response variables. However, it was not performed due to time constraints and the late reception of necessary data. This method description and lack of performance are relevant for further work into the spring of 2022.[14]

Gulpinar further found the dynamic response of the structure to be distinctly non-linear due to the drag-dependent damping. This implies that accurate results are best retrieved from a time-domain study. Gulpinar investigates this and finds around 10% increase in extreme heave motion for the time-domain approach. This provided evidence in favor of the time domain method, as it is more conservative from a ULS point of view. [14]

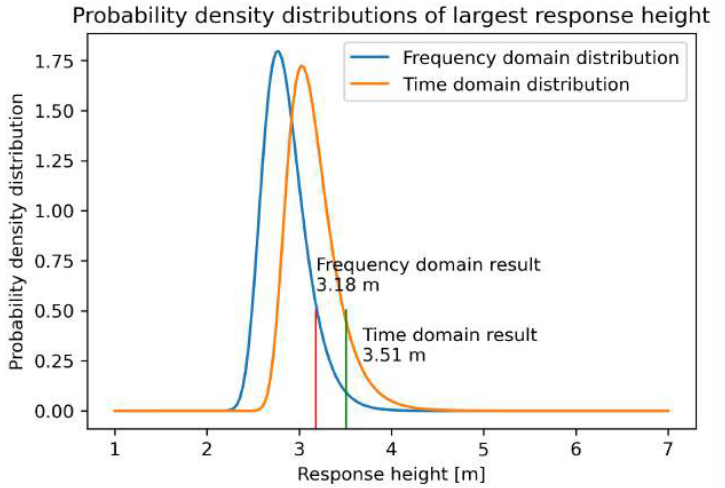

Figure 2: Gulpinars' comparison of Frequency and Time domain heave response [14]

1.2 Concept Description

Figure 3: Havfarm 1 in transport and after installation. From Nordlaks' website [22]

Havfarm 1 is owned by Nordlaks and is located approximately 5km off the coast of Hadsel. Approximately a 4th of its sectors are open, meaning sectors with an unhindered radius of 40km or above. The submerged structure looks similar to a ship's, while schematics reveal its semi-submersible principles. It is moored with eleven 22-ton anchors through a turret module, allowing it to rotate and move within a circle 900 m wide. This rotation will orient the bow toward incoming weather, yielding mostly head sea. The structure has service carts running on rails powered by electricity, acquired by cable from shore, with an additional backup generator for daily operations. The facility is operated by a double shift arrangement with six persons each.

It is a direct result of research licenses, of which they received 13 licenses (roughly 10 000 tons of fish) for phase 1 of the project. Nordlaks is investing approximately 4 billion NOK into the Havfarm projects. With the plan being two more structures, one can approximate a cost north of 1.3 billion NOK for the first phase. Currently, the capacity is 10 000 metric tons as the maximum allowed biomass. A salmon price of 60 NOK/Kg implies the project's potential for delivering 600 MNOK worth of fish in one cycle. At the time of writing this thesis, the application for a license transformation from research to regular licenses has been approved. Meaning the government has found adequate innovation and results documented for the project.

In this project thesis, the focus will be on the model developed by Vegard Holen. This means that the main bulk of data and dimensions utilized will be from calculations around the model itself. Thus some of the results will skew away from what can be considered realistic. The end report from Nordlaks and similar literature based on the specific structure will only be applicable for rough comparisons and not taken as the de facto answer to analyses performed.[16]

1.3 Rules

1.3.1 NYTEK

The current regulation regarding aquaculture is NYTEK, which states that the industry is to follow NS9415:2009 *Norwegian Standard for floating aquaculture*, or a comparable standard. The main criteria set by NYTEK is a proper safety level regarding fish escaping, which needs to be the same or higher than NS9415. For this purpose, DNVs *DNV-RU-OU-0503 - Offshore fish farming units and installations* is another applicable standard to follow. It is worth noting that NS9415 has been revised, awaiting NYTEK to be updated to reflect this change. NS 9415:2021 will, after said update, be the equivalent standard for aquaculture in Norway. [11][23][24][38]

1.3.2 NS9415 - Norwegian Standard for floating aquaculture

The motivation behind the NS9415 standard is to regulate aquaculture facilities to prevent fish from escaping. The updated 2021 version aims to include non-traditional aquaculture structures, such as the Havfarm concept. Both the old and new standard describes what approaches to use for several steps in the life cycle of an aquacultural production facility, from the project phase, installation and use. Roughly listed below:

- Estimation of environmental parameters and which ones to examine for a site
- What materials are used
- Main components: enclosure, floater, barge and mooring
- Component interaction
- Loads, load reactions and capacity calculations
- Extra equipment
- User manual (Including inspection and maintenance)

ULS The load-carrying members of the structure should be specified and their capacity documented. The design of steel floaters should, in general, according to NS-EN 1993-1-1 *Design of steel structures*, which to a large degree handles the required material characteristics and structural limits. A part of the ULS criteria is stated in the calculation and documentation of eigenperiods in surge, roll, and heave.

FLS The standard notes that the usual dimensioning service life is 20 years for fatigue. The standard states that a fatigue analysis should generally be based on SN curves based on experiments for the examined component. A dynamic load effect analysis is to be performed for the utilization of these curves. A consistent load case and SN-curve shall be employed for the Fatigue analysis. Finding any hotspot stresses in an FE-analysis shall result in the use of relevant SN-curves for evaluation. Reference for methodology is made to DNV-RP-C203 - *Fatigue design of offshore steel structures.*[36]

1.3.3 Applicable DNV Rules

DNV has a wide variety of rules depending on the structure type. As DNV covers a larger assortment of methods and cases, these rules will be the basis for calculations in this thesis. For this reason, a brief review of the most applicable rules for the Havfarm concept is to be presented in this section.

DNV documents are ordered by their purpose, represented in their abbreviations, of which the most relevant are:

- RU-OU - Rules for classification, Offshore Structures
- RP - Recommended Practices
- OS - Offshore Standards

DNV-RU-OU-0503 - Offshore fish farming units and installations cover a wide array of concepts. The rules document refers to what structural design standards to use depending on the structural characteristics and the design methodologies utilized. This rule document functioned as a reference document to other existing rules and recommended practices to be utilized in designing, verifying, and classifying a structure.

For the determination of design loads, the standard further references DNV-RP-C205 - *Environmental conditions and environmental loads*. A noteworthy difference from general offshore design practice is the DNV-RU-OU-0503 excluding environmental events with an annual probability lower than 10^{-2}, whereas NORSOK commonly operates with annual probabilities as low as 10^{-4}. This goes to show the extra precautionary level added when dealing with energy production on the Norwegian continental shelf.

DNV-RP-C205 - Environmental conditions and environmental loads guide design and operations. The recommended practice aims to deliver rational design criteria and methods to assess loads on structures affected by wind, waves, and currents.

To perform a ULS analysis on an offshore Structure, one must determine the wave conditions. For this, either deterministic design wave methods or applying wave spectra through stochastic methods can be utilized to describe wave conditions for structural design purposes. The approach is determined by what type of structure is analyzed and what response the structure exhibits.

A quasi-static structure response implies the applicability of deterministic design waves with characteristic wavelength, period, height, and crest height. Predicted with statistical analysis.

1.4 Transfer function Theory

From *DNV-CG-0130 Wave loads* the transfer function is defined: [40]

> The steady state solution x(t) of the equation of motions for linear theory can be written as:
>
> $$\boldsymbol{x}(t) = A \cdot \mathrm{Re}\left\{\boldsymbol{\eta}(\omega, \beta) \cdot \exp\left(i\omega_e t\right)\right\} \tag{1}$$
>
> A is the incident single wave amplitude of a regular wave of frequency, ω, from a direction, β. The corresponding encounter frequency is denoted as ω_e. The real part of a complex number is denoted as Re$\{\ldots\}$. The complex function $\eta(\omega, \beta)$ is the actual response-amplitude-operator RAO of response $\boldsymbol{x}$. Linear sea-keeping programs provide this function. Each component η_i of the vector $\boldsymbol{\eta}$ can always be expressed like this:
>
> $$\eta_i(\omega, \beta) = |\eta_i| \cdot \exp\left(i\theta_i\right) \tag{2}$$
>
> where $|\eta_i|$ is the amplitude of the corresponding component of $\boldsymbol{x}(t)$ in case $A = 1$. The actual response component will have a peak when:
>
> $$\omega_e t + \theta_i = 2\pi \cdot n \tag{3}$$
>
> Where n is an arbitrary integer, the real parameter θ_i is denoted by the phase of the response component.

This means a wave with the crest amidship corresponds to a phase angle of zero. Therefore, a further expected phase shift is about π or 180° when crossing the natural frequency.

Transfer functions are applicable for linear responses. This includes motions, accelerations, pressures, and loads calculated from these responses. A linear structural model can further establish transfer functions for stresses and strains at requested locations. However, it is not possible to establish accurate theoretical transfer functions for behavior that depend non-linearly on linear excitation.

1.5 Wave steepness

From the DNV-RP-C103 Column-stabilised units document, there are set steepness criteria. In addition, desired design wave characteristics are described as having a reference wave height for a specific location being the 100-year wave, H_{100} The wave steepness is defined below in Equation 4 and the limit set by it in Equation 5.

$$S = \frac{2\pi H}{gT^2} \tag{4}$$

$$S < \begin{cases} \frac{1}{7} & \text{for } T \leq 6s \\ \frac{1}{7+\frac{0.93}{H}(T^2-36)} & \text{for } T > 6s \end{cases} \tag{5}$$

The max wave height expressed through the steepness limit is then given:

$$H = \begin{cases} 0.22T^2 & \text{for } T \leq 6s \\ \frac{T^2}{4.5+0.6/H_{100}(T^2-36)} & \text{for } T > 6s \end{cases} \tag{6}$$

1.6 Wave and current loading for in USFOS

Different theoretical wave foundations will be utilized for analytical purposes depending on which case is examined. The airy wave theory will be applied to examine the linearity of the problem and develop transfer functions.

1.6.1 Force model - Morrison Equation

The Morison equation, Equation 7, can be used to calculate the wave and current loading on the bow section of the structure. As seen in Figure 4 it describes the horizontal force acting on a strip along a circular member.

$$dF = \rho \frac{\pi D^2}{4} C_M \dot{u} dz + \frac{1}{2} \rho C_D D u|u| dz \tag{7}$$

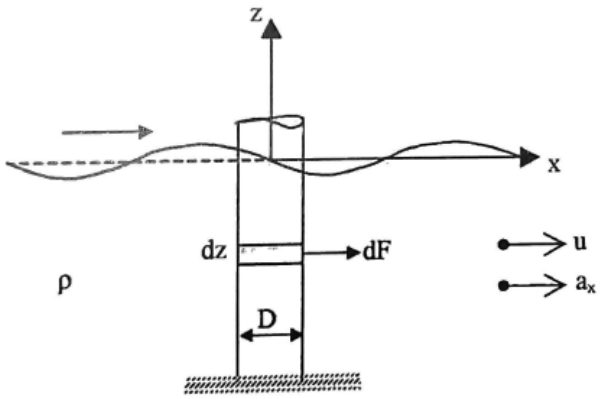

Figure 4: Morison equation with positive wave propagation toward the right [28]

ρ being the density of water, D the cylinder diameter, u the horizontal water particle velocity, $\dot{u}(= a_x)$ horizontal water particle acceleration at the midpoint of the strip. Mass and drag forces are scaled through C_M and C_D, empirically determined coefficients. One of the force types will typically dominate. It is, therefore, relevant to examine what domain one is operating within. To determine this one can utilize Figure 5 as a guideline. [28]

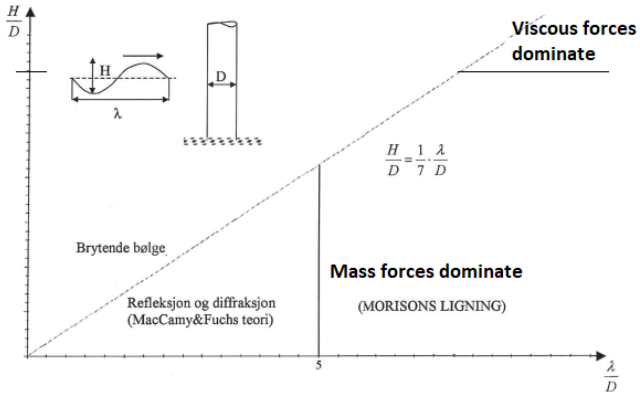

Figure 5: Overview of Morisons' applicable regimes [28]

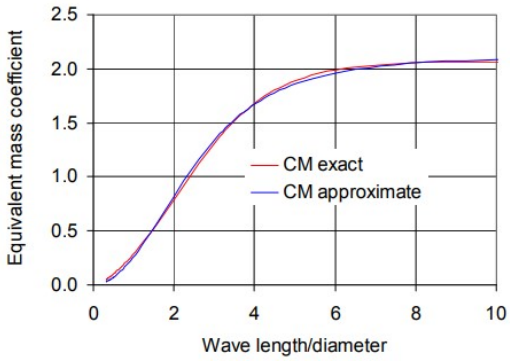

Figure 6: Equivalent mass coefficient [32]

As this is the force on a stationary cylinder, one needs to consider two aspects further:

- Not all structural members are cylinders
- Calculation for structural members moving relative to the wave particles

1.6.2 Morrison applied to non-cylindrical members

The equivalent mass coefficient can be expressed through the Mac-Camy and Fuchs force as per Equation 8.[32]

$$C_M^{eq} = \frac{4}{\pi} \frac{A\left(\pi \frac{D}{\lambda}\right)}{\left(\pi \frac{D}{\lambda}\right)^2} \tanh\left(2\pi \frac{d}{\lambda}\right) \tag{8}$$

This gives a good approximation for the mass coefficent as function of the relation between wavelength and element diameter. This is visualized from the USFOS hydrodynamic theory documentation, see Figure 6.

As for the actual implementation in the previous models, this is implemented through a constant $C_M = 1.68$ for box sections and $C_M = 1.2$ for pipe sections. Seeming quite reasonable for the later proved influential 4 second period considering a 4-meter diameter and a .

1.6.3 Morrison for moving structural members

The non-cylindrical structural members are accounted for through the mass and drag coefficients, C_M and C_D. The implementation of this in the model will be similar to Holen's approach in 2017. [16]

To account for the relative movement between a part of the structure and an arbitrary wave, the effect of relative structural motions is included in each term of the Morrison equation. Done by finding the relative velocity and acceleration of the structure with respect to the incoming wave through iteration. [32] This relative particle velocity with respect to the structure can be represented as:

$$\mathbf{v}_{rn} = \mathbf{v}_n - \dot{\mathbf{x}}_n \tag{9}$$

Here $\mathbf{v}_n$ is the wave particle velocity and $\dot{\mathbf{x}}_n$ is the velocity of the model section in question. By perfroming this calculation for all three translational dofs, the relative velocity of a wave particle becomes:

$$v_{rn} = \sqrt{v_{xr,n}^2 + v_{yr,n}^2 + v_{zr,n}^2} \tag{10}$$

This is an optional calculation in USFOS and must be specified by inputting the REL_VELO record into the control file. The calculation transforms the structure velocity to an element's local axes and subtracts the local wave velocities. [32]

1.6.4 Load applicability

The load calculation will be done through USFOS. Since it is a non-linear structural finite element solver, several theories are also available for hydrodynamic load application. The theories yield differences regarding the free surface and forces acting on a structure. From linear theory, that has no difference in the crest and trough amplitude and no drift forces. To higher-order wave theory resulting in free surface amplitude differences and drift forces. The differences between these theories will affect their applicability in the wanted utilization. Thus it is crucial to know their up -and downsides. To help with this the USFOS hydrodynamic theory booklet illustrates the application regimes of the different theories.[32]

- Linear (Airy) wave theory for infinite, finite and shallow water depth
- Stokes 5th order theory
- Dean's Stream function theory
- "Grid wave" – Flow kinematics found through computational fluid dynamics

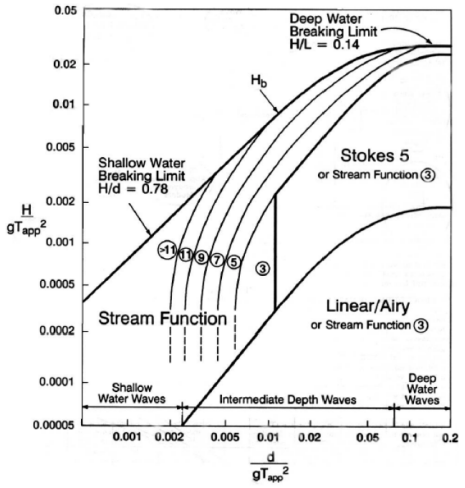

Figure 7: Regimes of applicability for wave theories [32]

Looking at Figure 7 one can, by a quick evaluation of the wavelength, evaluate what regime one should operate within when applying wave theories. Further, in DNV-RP-C103, 2.2.5 Wave theory, it is stated that airy waves provide sufficient accuracy for column-stabilized units. This is due to the wide variety of applicable regions regarding depth. Furthermore, the airy wave application results yield satisfactory results even when diverging considerably from the small wave height assumption the linear theory is based upon. [35]

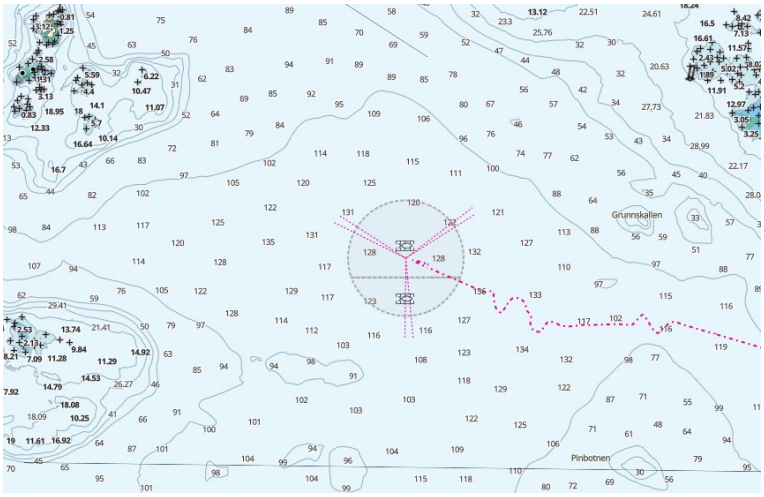

Figure 8: Cutout of sea map describing the sea floor conditions around Havfarm 1[3]

From the sea map included, one can observe that the depth at the current Havfarm1 1 location is approximately 130 meters, coinciding with what has been used to evaluate the Havfarm structure in the previous master thesis on the subject, written by Gulpinar. From the literature, we know that deep water application can be simplified to having $2 * \pi/k > 1/2$. Applying deep water conditions is thus valid while the depth is less than double the wavelength. For the specific location of Hadsel, this yields deep water conditions for wavelengths up to $\underline{\lambda = 260 meters}$. Establishing that regular waves with periods up to 12 seconds is within deep water conditions. Further, it should be noted that some of the motivation behind this master thesis is the evaluation of the dynamic Havfarm concept in exposed waters, making it reasonable to assume deep waters. [28]

1.7 Wave loading - JONSWAP spectrum

The JONSWAP spectrum, given in Equation 11, is a special case of the Pierson-Moskowitz spectrum. It will serve as a basis for the irregular sea simulations to be performed in this thesis, based on recommendations for stochastic simulations in DNV-CG-0130. [40]

$$S_{JS}(\omega) = A_\gamma \frac{5}{16} \cdot H_s^2 \omega_p^4 \cdot \omega^{-5} \exp\left(-\frac{5}{4}\left(\frac{\omega}{\omega_p}\right)^{-4}\right) \gamma \exp\left(-0.5\left(\frac{\omega - \omega_p}{\sigma \omega_p}\right)^2\right) \tag{11}$$

1.8 Havfarm 1 Metocean report Ytre Hadseløya

In the end report for the first cycle of Havfarm 1, there is appended a metocean study conducted by MutliConsult. [3] In this report, they describe the establishment of a contour line plot for a more exposed location and thus have a conservative foundation for structural ULS compliance evaluation.

1.9 Hindcast contour plot from location

In the summary report from the first deployment of Havfarm 1, a contour plot based on hindcast data for the location is provided. [3] This plot allows the choice of sea states of particular interest, which is to be compared to the results from the establishment of the transfer function.

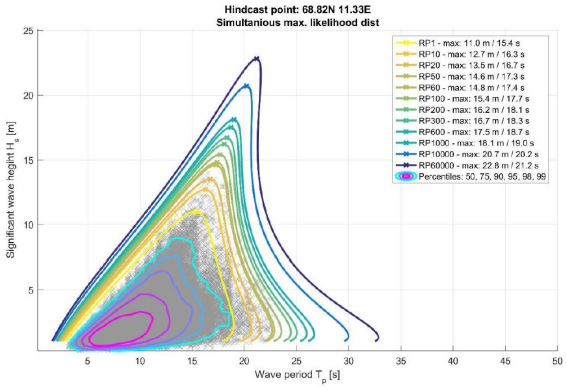

Figure 9: Contour Line plot for H_s and T_p.[3]

The contour plot above is based on an extreme value analysis performed by MultiConsult, of hindcast data from the WAM10 model provided by the Norwegian Meteorological Institute. The dataset covers 60 years, 1957-2017, with a 3-hour resolution for the sea states. The exact location of the wave point for the WAM10 data set and Havfarm 1 is marked in Figure 10. [3]

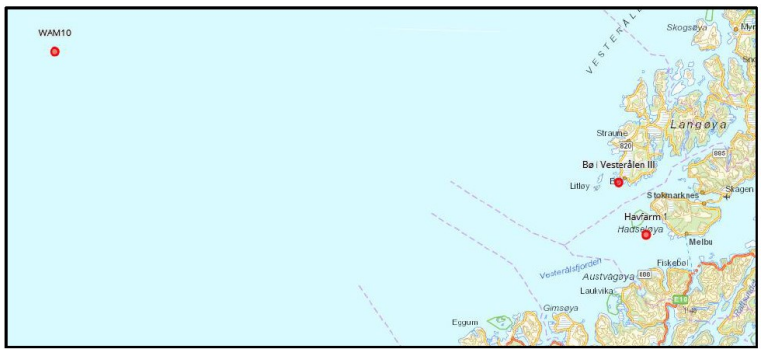

Figure 10: Map showing WAM10 wave point, Havfarm 1 location and Bø meteorological station , all marked in red.[3]

Assuming this wave point to represent the conditions that Havfarm 1 is exposed to might introduce an error. However, this error should be sufficiently conservative, considering the structure is placed in a more sheltered environment compared to the measuring point.

1.9.1 3-parameter Weibull distribution

The 3-parameter Weibull distribution is given by Equation 12. A common practice for retrieving the Nth response percentile is to fit a response data set to this distribution and then calculating the probability of response exceedance for said responses.

$$f(x) = \frac{\beta}{\alpha}\left(\frac{x-\gamma}{\alpha}\right)^{\beta-1} e^{-\left(\frac{x-\gamma}{\alpha}\right)^{\beta}} \tag{12}$$

1.9.2 Contour line methodology

In Multiconsult's approach, the contour plots' distribution of H_s and T_p is done through the Conditional Modelling Approach (CMA), described in DNV-RP-C205. H_s is assumed to be Weibull distributed, estimated according to (Mathisen Bitner-Gregersen, 1990). Mathisen et al. recommend combining a marginal 3-parameter Weibull distribution for significant wave height with a conditional log-normal distribution for the zero-up-crossing period. [19] [3]

$$f_{TpHs}\left(T_p, H_s; \alpha, \beta, \gamma, a_1, a_2, a_3, b_1, b_2, b_3\right) = \frac{1}{T_p\sqrt{2\pi}\epsilon_{Tp}(Hs)} \exp\left\{-\frac{\left(\ln\left(T_p\right) - \xi_x\left(H_s\right)\right)^2}{2\epsilon_{Tp}^2(Hs)}\right\} \cdot \frac{\beta\left(H_s-\gamma\right)^{\beta-1}}{\alpha^{\beta}} \exp\left\{-\left(\frac{H_s-\gamma}{\alpha}\right)^{\beta}\right\} \tag{13}$$

With $\xi\left(H_s\right) = a_1 + a_2 H_s a_3$ and $\epsilon\left(H_s\right) = b_1 + b_2 \exp\left(b_3 H_s\right)$

The marginal Wibull parameters α, β and γ are determined through the nonlinear least square method. By grouping the significant wave heights, the detemination of $\xi(H_s)$ and $\epsilon(H_s)$ for the distribution of zero-upcrossing period T_z is possible. From this, the $a_1, a_3, a_3, b_1, b_2, b_3$ are determined.

In establishing the contour lines, a Constant probability density is assumed. Through this assumption and assuming H_s to be Weibull distributed, the extreme values for significant wave heights corresponding to different return periods are found. From the Extreme value theory surrounding the generalized extreme value distributions, the limit function of extreme maximums of a Weibull distributed value is given to be Gumbel distributed. [4] Thus, the annual max wave height can be assumed Gumbel distributed. The method of moments is then utilized to find the Gumbel parameters.

The Gumbel distribution itself is given by:

$$F_c\left(H_s\right) = \exp\left\{-\exp\left[-\frac{\left(H_s-U\right)}{A}\right]\right\}, \tag{14}$$

Distribution parameters A and U relate to the standard deviation $\sigma = 1.283$ Aand mean $\mu = U + 0.557$ A of the Gumbel variable. The median T_p is calculated from the estimated extreme H_s. The contour of the constant probability from the CMA model through a combination of extreme H_s and conditional T_p.

1.9.3 Individual max wave height

MultiConsult calculated the wave height maximum with a return period of 100 years. The calculation of this is based on the contour line approach and follows DNV-RP-C205 Environmental conditions and environmental loads, section 3.5.9 *Short term distribution of wave height*. In the recommended practice, the short term wave height distribution is given by the Weibull distribution conditionally given through H_s:

$$F_C(x) = 1 - \exp\left[-\left(\frac{x}{\alpha_c H_s}\right)^{\beta_c}\right] \tag{15}$$

The scale and shape parameters given to be $\alpha_H = 0.681$ and $\beta_H = 2.126$ from the Forristall distribution. For a 3-hour sea state, the maximum individual wave height is calculated as the Nth power of Equation 15. N corresponds to the number of waves during the sea state, found through the first moment of the wave spectrum T_{m01} (also known as the mean wave period). Further, the individual wave height for larger return periods is approximated through the 90th percentile of the calculated short-term distribution. MultiConsult found this to be 11.8 meters. [3] The corresponding wave period is given in DNV-RP-C205, section 3.7.4.2, and can be calculated as:

$$T_{Hmax} = \alpha \cdot H_{max}^{b} \tag{16}$$

With the empirical coefficients $\alpha = 2.94$ and $b = 0.5$ for the Norwegian continental shelf. Giving a wave period of 10.1 seconds.

2 Model Adjustments and Eigenvalues

Vegard Holen established a model for analysis of the Havfarm concept. An observation made regarding his model is that the yield utilization factor is substantially lower than expected. In the discussion, it is pointed to several modeling choices, possibly introducing errors.

Without the net included, the pure structural model will be further investigated regarding necessary adjustments for obtaining realistic responses to analyze. Regarding this thesis' scope, model changes will be made to obtain meaningful results for the requested deformation modes.

It is important to consider that the thesis is written as an academic exercise and does not aim to evaluate the actual Havfarm 1 structure precisely. Instead, the purpose is to further the author's understanding of such an evaluation and study how to achieve conservative estimates reliably. For this process, the concept will be evaluated through a simplified model. Model changes are approached to improve modeling skills and study the theory behind them and their effects. With that being said, the similarity is apparent, and it is relevant to compare results with what the analyses performed on the actual structure yielded.

2.1 Holen's model

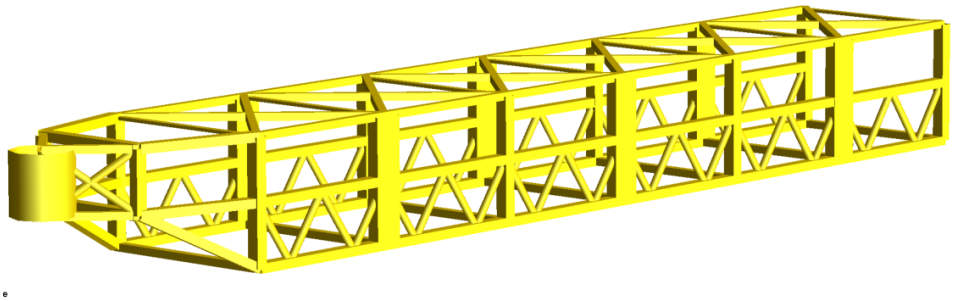

Figure 11: Vegard Holens' Havfarm USFOS model

The model is composed of stiff beam elements, making up six longitudinal pontoons, of which the lower four will be the main contributors to the buoyancy. Transversely it is stiffened by seven girders parting up the structure for its six net pens and co-axially stiffened by diagonal joint-connected braces over each net pen. The bow section is modeled to yield large forces to account for the missing lice skirts in the model. To achieve this, the bow section included a 20-meter wide pipe. This inevitably introduced an unrealistic buoyancy force and made the pitch motion unrealistically large. This interfered quite a bit with Holen's and Gulpinar's heave results. In addition, a large portion of their time series had to be discarded as the transient motion of the structure was large and was not adequately damped before well into each simulation.

Holen aimed to achieve the initial design steel weight estimates, 34 000 metric tonnes, provided by NSK Ship Design. Making the model slightly lighter than the finished structure at 37 500 metric tonnes. The cross-sectional dimensions were calculated based on the initial rough estimate. The modeling choices were using equivalent thickness for the entire

length of the structural members or modeling according to structural drawings. It is stated there were no detailed drawings available, and thus the stiffeners' weight was modeled as smeared with constant cross-sectional dimensions for the entire element lengths. [1][16]

A schematically accurate model would yield more accurate joint stresses, which would be usable in an FLS analysis of the structural sections. Such a model adjustment is not planned as an FLS analysis is beyond the scope of this thesis. Focusing on global ULS analysis reduces the importance of the accuracy of stresses in the joints. [16]

Table 1: Model & structure dimensions. [16] [22]

Dimension	USFOS Model	Structure
LoA[m]	396	385
Height[m]	40	37.75
Width[m]	60	59.5
Operational draft[m]	30	37.75
Weight $[10^3 kg]$	34 290	37 500

Holen initially intended to model the mooring forces through the catenary equation and is part of the reasoning behind the large bow buoyancy element. The catenary approach proved difficult and time-consuming to implement and introduced numerical instability in the 3-hour run. The end result became a spring-modelled mooring application through a horizontal *1 Node Spring to Ground* with stiffness of 400 $\left[\frac{kN}{m}\right]$. This spring introduces a rather large horizontal stiffness and is due for investigation. It also makes the surge eigenperiod non-realistic until the spring is properly calibrated, as the eigenperiod of the system relies significantly on the spring introduced.

2.2 Model modifications

The first task at hand for this thesis is adjusting the model to fit the real structure better while still keeping to the simplified approach. The reasoning behind the simplification of the structural model is both based on reducing computational demand and making hand calculations more feasible.

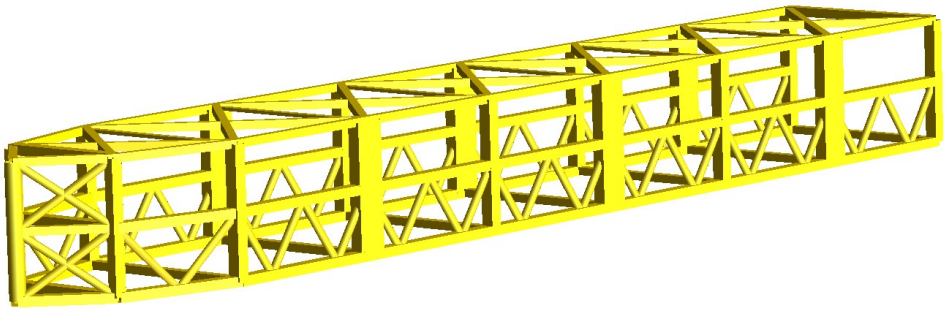

Figure 12: Adjusted model

2.2.1 Modification of bow section

In an attempt to model the bow section more realistically, the pipe diameter was reduced to 5 meters. Further, the entire section was continued down to the global draught of 30 meters, or 40 meters.

This will reduce the intense pitch motion during the simulations to be run, especially beneficial when performing natural period decay tests. Gulpinar recognized this problem and removed the bow section for a separate series of decay tests. He also had the large nodal masses implemented quite close to the bow. It was decided early in the project timeline that decreasing this longitudinal imbalance was of great interest regarding the accuracy of structural response analysis.

Adjusting the bow pipe radius from 10 to 5 meters, then extending its draught to 40 meters, yields a significant structural change. However, the weight will be small compared to the reduced buoyancy. This can be seen in that the steel volume, thus material weight, of a cylinder is linearly affected by a radical change. In contrast, the enclosed volume giving buoyancy is quadratically affected.

The change is twofold, as while decreasing the cylindrical element, it is also extended 20 meters further down to -30 meters from the free surface. Additionally, the supporting framework is extended to the same draught, adding more buoyancy elements and steel weight. In total the additional elements weigh 1342079$[kg]$, corresponding to a 4.29% mass increase. The total reduced buoyancy is 829.9$[m^3]$, a 2.6% reduction in buoyancy. Calculations for is found in the appendix.

2.2.2 Mass implementation

In addition to modeling the weight through the cross-sectional properties, 1100 metric tons of the structural weight was modeled as concentrated mass. An important detail regarding the NODEMASS function is its inputs for mass, being a concentrated mass in the x, y, and z-direction. Additionally, it takes on rotational mass around the x, y, and z-axis. After further consultation, the mass must be defined for all 3 translational dofs and rotation around each axis. Especially relevant for simulations such as torsional decay, dynamic response, and flat wave spectrum response. After continuing the bow section down to the global draught of 30 meters and flooding some additional compartments, the relation between COB and COG was changed. This led to the necessity of moving the COG slightly back by redistributing the nodal masses.

Table 2: Nodal mass distribution

Node	Modified [10^3kg]	Original [10^3kg]
1000/2000	275	90
1008/2008	250	0
1024/2024	300	200
1040/2040	200	810

2.3 Eigenperiod estimation

When a system is excited with a cyclical load close to its natural frequency, it will yield an amplified response relative to any other frequency region. In the cases of sea waves, the response may become significantly more significant than the displacement of the free surface itself. This phenomenon is called resonance. Therefore, estimation and control of natural periods are of the utmost importance when designing Marine structures. For the rigid body motions (RBM), there has been extensive work performed in earlier theses, subject to control for the adjusted model. Further, the focus in this thesis is shifted to the global structural deformation modes, such as hull bending and torsion.

This section will cover the estimation of these periods for the important modes a structure can oscillate in. Although surge is specified in NS:9415, it is neglected in this section as it is controlled largely through the mooring, which is modeled through simplified springs here. In reality, mooring implementation requires a far more comprehensive modeling approach, such as implementing the catenary equations before one can accurately evaluate its influence.[13]

A point worth noting when comparing the calculations to earlier theses is the width of the structure. Holen stated the width was 60 meters. [16] However, with closer inspection of the model code, one can observe that there is 60 meter spacing between nodes, which themselves are at the center of the 4-meter wide pontoon elements. Making the final width 64 meters, affecting stability and natural period calculations, as the water plane area moment of inertia is quadratically affected by the distance from the centerline, seen in 18 and Equation 19. Simple calculations made in this section are found in Appendix A

2.3.1 Eigenperiod estimation for heave

Heave is a tremendously important response variable, and its range can be predicted based on the structure type and its characteristic dimensions. Categorizing the structure as semi-submersible yields the target design's natural heave period above 20 seconds. [9]

Estimation of natural periods requires knowledge of the structural mass and corresponding added mass. After adjustment, the model weighs 34 283 metric tonnes. Equation 17 requires the water plane area and added mass in heave.

Faltinsen states that the undamped natural period in heave for a freely floating structure is done through Equation 17. [9]

$$T_n 3 = 2\pi \sqrt{\frac{M + A_3}{\rho g A_w}} \tag{17}$$

2.3.2 Eigenperiod estimation for roll

In *DNV-RP-C205* it is stated that the typical roll/pitch period for a semi-submersible is 30-60 seconds, and outside typical excitation ranges for sea states given in Section 1.8. However, these "typical" structures do not have such a large length to width ratio, and it is of interest to further investigate this. From Faltinsen, it is known that the undamped natural period in roll can be found with Equation 18. [9]

$$T_{n4} = 2\pi\sqrt{\frac{Mr_{44}^2 + A_{44}}{\rho g \nabla \overline{GM}_T}} \tag{18}$$

Transverse stability of a ship is given from the relations in Figure 13

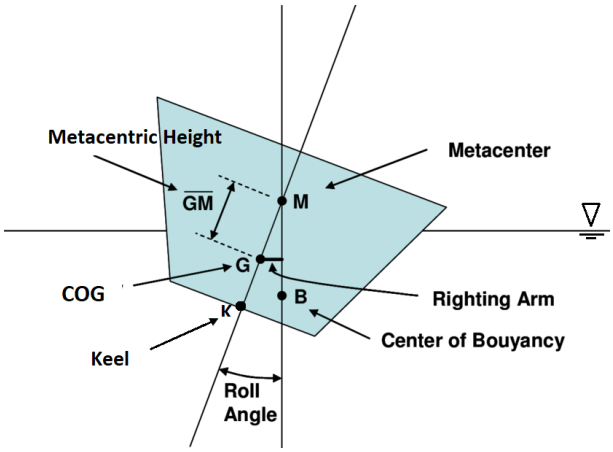

Figure 13: Charecteristic points defining transverse stability of a freely floating body

From Figure 13 it can be seen that transverse Metacentric heigh, $\overline{GM}_T$, is given by:

$$GM = KB + BM - KG \quad , \qquad BM = \frac{I}{\nabla} \tag{19}$$

2.3.3 Eigenperiod estimation for vertical bending

The bending mode natural period is should not be of significant influence for semi-submersibles. However, due to the beam-like dimensions of the Havfarm concept, it is deemed valuable to evaluate.

From *An Introduction to Shock Vibration Response Spectra, By Tome Irvine* one can find one approach for developing the natural frequency formulation for a free-free beam. Equation 20 is the governing equation for beam bending free vibration and can be used to describe the oscillatory behavior of a free beam. [6][18]

$$-\frac{\partial^2 y}{\partial x^2}\left[EI(x)\frac{\partial^2 y}{\partial x^2}\right] = \rho_L \frac{\partial^2 y}{\partial t^2} \tag{20}$$

Assuming constant bending stiffness over the beam length, the equation 20 can be expressed with a simplified stiffness expression, EI.

$$-EI\frac{\partial^4 y}{\partial x^4} = \rho_L \frac{\partial^2 y}{\partial t^2} \tag{21}$$

$$y(x,t) = Y(x)exp(j\omega t) \tag{22}$$

$$\frac{\partial^2}{\partial t^2}y(x,t) = -\omega^2 Y(x)exp(j\omega t) \tag{23}$$

Through the separation of variables and substitution into 21, one can express the governing equation for beam bending as a spatially ordinary differential equation, Equation 24. [6]

$$\frac{\partial^4}{\partial x^4}Y(x) - \omega^2\left\{\frac{\rho_L}{EI}\right\}Y(x) = 0 \tag{24}$$

With the substitution $\beta = \omega^2\left\{\frac{\rho_L}{EI}\right\}$ the spatial solution can be expressed as:

$$Y(x) = a_1\sinh(\beta x) + a_2\cosh(\beta x) + a_3\sin(\beta x) + a_4\cos(\beta x) \tag{25}$$

$$\begin{aligned}\beta^4\{a_1\sinh(\beta x) \; &+a_2\cosh(\beta x) + a_3\sin(\beta x) + a_4\cos(\beta x)\} \\ &-\omega^2\left\{\frac{\rho}{EI}\right\}\{a_1\sinh(\beta x) + a_2\cosh(\beta x) + a_3\sin(\beta x) + a_4\cos(\beta x)\} = 0\end{aligned} \tag{26}$$

Finally, this can be solved for ω_n and solved for the boundary conditions. The subscript n indicates what mode is evaluated, which will be the lowest. As the structure is free-free, the end deflection and moments are zero, meaning that the relative translation will be the beam itself that deflects between the ends.

$$\omega_n = \beta^2\sqrt{\frac{EI}{\rho_L}} \tag{27}$$

$$Y(0) = Y(L) = 0, M(0) = M(L) = 0 \tag{28}$$

Tom Irvine solves this case in *Bending Frequencies of Beams, Rods and Pipes, Revision T.*[17] The natural frequency for a free-free beam can then be calculated with Equation 29. [17]

$$f_n = \frac{1}{2\pi}\left[\frac{22.373}{L^2}\right]\sqrt{\frac{EI}{\rho_L}} \tag{29}$$

Depending on the assumed length of the structure, (i.e., the net pens or entire length), the frequency changes. Of course, the inverse relation of this change will remain true for the resulting period. With a length of 336m and 396m the Natural Bending Period comes out to 0.82 and 1.05 seconds respectively.

2.3.4 Identification of favourable wave period for torsion

After several failed attempts at calculating the natural period in torsion for the structure, the next best thing is proposed. Thus a rough estimation of a potential problematic period for the system might be found through wave length in relation to the structures dimensions. Consider an oblique wave incoming at a 45 degree angle. The wave length corresponding to a wave crest being at one transverse side of the structure, and a wave trough being at the other transverse side, is given by:

$$\lambda_n = cos(45) \cdot w/2 \tag{30}$$

with a width of 60 meters, this gives a wavelenght $\lambda = 21.2[m]$. The period for this corresponding wavelength can now be calculated through the relation:

$$T = \sqrt{\frac{2 \cdot \pi \cdot \lambda}{g}} \tag{31}$$

With $g = 9.81[m/s^2]$, this results in a period of 3.68 seconds. Of course, it is merely a quick estimation to point wave periods to consider. Changing the angle would give completely different results. However, imagining an integral over all the incoming wave angles where the force exciting torsional deformation is expressed as a function of angle, the largest contributions would have to come from oblique waves. Further the smallest contributions would have to stem from the all cardinal directions (0,90,180 and 270 degrees). The proposed integral would have somewhat agree with the structural eigenperiod found in later decay tests.

2.3.5 Assumptions made

- Added mass will be equal to mass structure
- Radius of gyration in roll can be aproximated as $r_{44} = k = \sqrt{I/A} = 20.7[m]$
- The contribution from the pipe in the bow is negligible
- Structure can be modelled as a uniformly stiff beam in bending
- Evenly distributed mass over beam/structure length

2.3.6 Eigenperiod estimation through decay testing

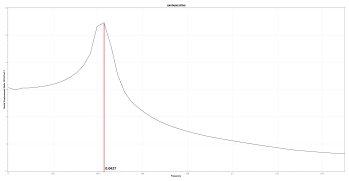

(a) Heave decay over frequency

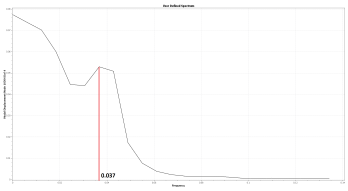

(b) Roll decay over frequency

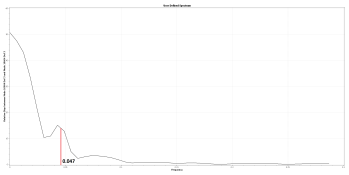

(c) Pitch decay over frequency

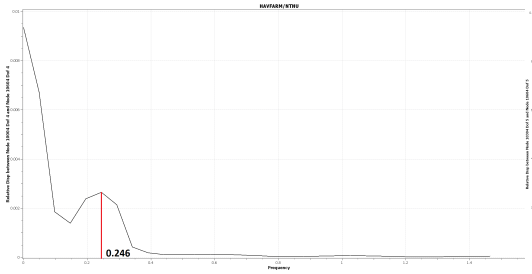

(d) Torsion decay over frequency

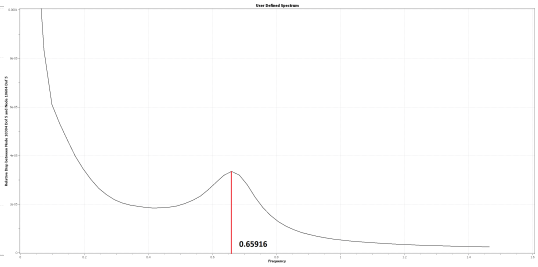

(e) Bending decay over frequency

Figure 14: Decay test plots for frequency response

Table 3: Natural periods tabulated

Mode	Tn Calculated [s]	Tn Decay [s]	% diffference
Heave	22	23,4	-5.98
Roll	[35,8-40,2]	27	32.5
Pitch	-	21,3	-
Torsion	3.68	4,07	-9.58
Bending	[0,82-1,05]	1.52	-30.1

2.4 Discussion

The wavelength chosen to evaluate the applicability off implemented mass coefficients is chosen based on the eigenvalue for torsion, as the largest focus is to be put into this mode. As briefly discussed Section 1.6, the value seems to be quite accurate for this region. It might however underestimate the force for larger wavelengths.

The rough estimates for the eigenperiods align adequately for Heave and Bending. For the roll eigenperiod, the error became quite large, overestimating it by over 30%. This is to large degree due to the difficulty of establishing the radius of gyration for such a slender and "empty" structure. The same percentile error is to be found in the bending calculation, tough the error is low in absolute terms, thus a valid ballpark estimate for an analyst to further consider the surrounding period region.

The investigation into problematic wave periods for torsion was extremely simplified, but seems to yield a valid result to consider. However it cannot be overstated that this is not a eigenperiod calculation. It does not consider the stiffness of the structure. For further work, this calculation should be explored in an attempt to invalidate it.

3 Transfer Function

The transfer functions to be established visualize the response over wave height for different periods. Especially expected hull bending at around 1 second and torsion around 3-4 seconds. The range for torsion is based on the results obtained from decay tests in Section 2.3 and 7Waves' sensor data for Havfarm 1 where they reported an eigenperiod of 3 seconds for the torsional mode.[3] These results give a foundation to compare the simulations and the resulting transfer function. Here, it should be noted that the model utilized is severely simplified compared to the real structure in this thesis.

3.1 Method for establishment of arbitrary transfer function

In Section 1.4 the analytical approach to transfer functions has been described. However, the establishment in this thesis will be performed through simulation of the relevant motion desired.

A practical approach to establishing the transfer function is performing many simulations for different wave heights. It was implemented through the application of airy single wave theory. This should provide a response function for unit loads.

The structure should be subjected to a flat wave spectrum to express the dynamical response. The difference between the response for this spectrum and the different single waves will give the transfer function for the structure.

3.1.1 Simulations and post processing

There are some simulations to achieve results with linear response contributions where the wave height is kept low, specifically 0.1 and 1 meter. Further, the accuracy of linear response prediction is to be investigated through this thesis. For this, the wave heights of 6 and 10 meters will be utilized and compared to the expected linear responses.

The simulations themselves are kept going for as long as required to eradicate as much transient motion as necessary to not interfere with the torsional response itself. The relative roll response shall be established for each run from these simulations. Further, this response should be evaluated as a function of either period or frequency and plotted as such.

USFOS is run through a python script that initializes the USFOS executable directly with inputs specified in the same code. This includes the modified model.fem and head.fem file containing the wave load information and what results to save to the .dyn file. Another script then processes this, using the Dynres executable to produce a time-series of desired responses.

In his thesis, Gulpinar found the heave transfer function for the unmodified model through a similar method.[14] For this, the period range was implemented through a constant period-step. This leads to the same period step between 3 and 4 second wave periods as 10 to 11. However, as the relative difference is inversely dependent on the period, one wants to have a smaller step length for smaller periods. This is especially true when looking at motions with expected low natural periods, as the aforementioned results from the decay simulations and 7waves' report indicate.

As the model has been further improved in the previous iteration, its initial conditions are closer to even keel. Thus the time required to dampen out transient motion is reduced. The improved initial conditions allow the discard time, the period before collection of responses, to be reduced from 300 to 200 seconds. Resulting in a far less computational demanding set of simulations. Further computational efficiency is achieved through the simple fact that the periods are approximately 8 times smaller, requiring significantly less run time to obtain a sufficient amount of oscillations.

For each wave height, there were run between 25-100 simulations, depending on the desired resolution in the change of the circular frequency (and resulting period). These runs were then evaluated through a self-produced post-processing script (see appendix). Here the max amplitude of Relative roll between bow and aft after the discard time was plotted for the respective period of the simulation. These were then divided by their respective wave height to obtain a unit wave response function.

For the flat spectrum response simulation of the structure, Tore Holmås was consulted. After his help in altering the prepared user-defined, constant area, flat wave spectrum, a 30-minute simulation of said spectrum was ran. The same response as obtained from the airy wave simulations was Fourier transformed to a response-frequency function. This response spectrum was subsequently subtracted from the response spectrum obtained through airy single waves, thus yielding a transfer function.

After the approach for establishing the torsional transfer function was developed, the same methodology was applied to examine global bending. This was achieved by retrieving the relative roll between aft and bow around the y-axis instead of the x-axis as performed regarding torsion.

Lastly, the transfer functions have to be interpolated. This is done with reasoning from DNV RP C205: "Transfer function should be smooth and describe the behavior to a wide range of states." [37] More aptly done with interpolation to fit the periods not simulated.

3.1.2 Nodal locations utilized in the analyses

When mentioning the fixed nodes, there are two nodes mainly being utilized. Visually presented here.

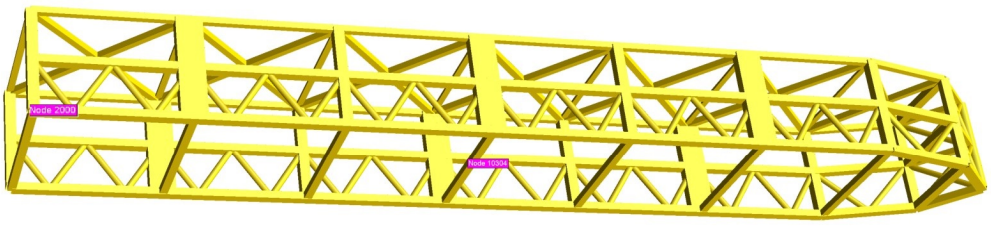

Figure 15: Aft and middle bottom node, 2000 and 10304 respectively

3.2 Dynamic response

The structures' response to single wave spectrums with varying periods is presented below. This means that sinusoidal waves are sent at a 45-degree angle to the structure for each period. The torsional response being referenced is the relative roll response in radians of the aft and front bottom pontoon nodes of the net pen section. As far as expectations go, the structure is expected to experience a significant degree of dynamic responses; thus, increasing the wave height should not yield linear responses. Whether this will be the case is to be observed.

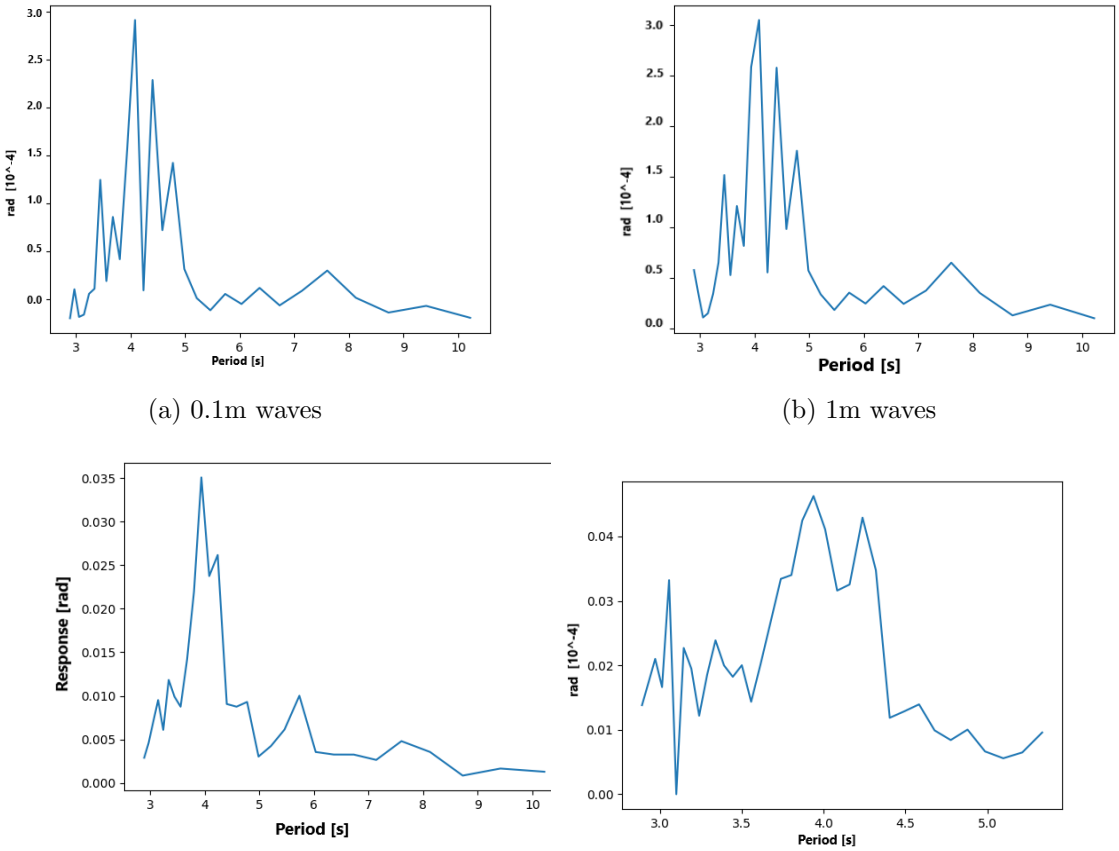

(a) 0.1m waves

(b) 1m waves

(c) 6m waves

(d) 10m waves

Figure 16: Relative roll response aft-bow, dynamic

As one can see from Figure 16 the response follows a linear trend going from 0.1 to 1-meter wave height. Surprisingly this seems to be the case going to 10 meters as well. However, the 6-meter case partially contradicts the linear response development here.

A caveat for the larger airy waves utilized for the 6 and 10-meter response spectrum is the wave steepness. As provided in Equation 4, the maximum wave steepness can be evaluated through Equation 6. For a 6-meter wave, this calculation yields a minimum period of 5.2 seconds for the case to be valid. This might explain some of the non-linear development of the response spectrum.

3.3 Static response

For the static analysis, a bottom node (Node 10304) close to the middle of the structure is fixed; see Figure 15. The choice of location for the fixed node is motivated by a desire to reduce the effect of the global roll moment on the relative displacement of the nodes.

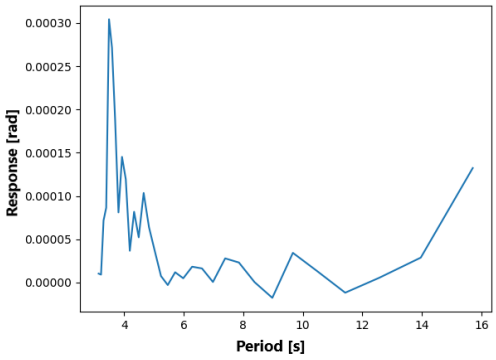

(a) 0.1m waves

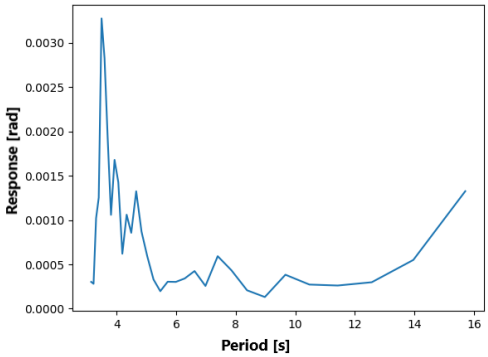

(b) 1m waves

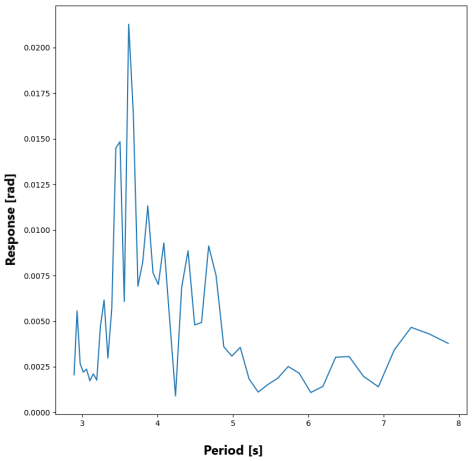

(c) 6m waves

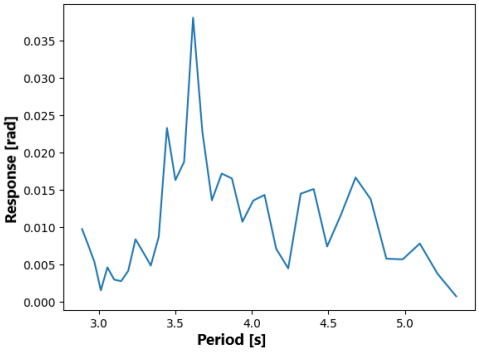

(d) 10m waves

Figure 17: Relative roll response aft-bow, Static

The resulting responses makes sense. The decreased response amplitude can be explained by the spring fixed node receiving some of the torsional energy. The consistent but slightly lower peak response period corresponds to an increase in stiffness for the structure, introduced by the spring. Further the static results seem to conform to the linear response when increasing wave heights, as seen in the dynamic configuration.

3.4 Other effects

During the establishment of the torsional transfer function, several other effects of the initial conditions revealed themselves. These effects are shortly discussed in this subsection.

3.4.1 Water plane stiffness

For the static analysis, the effect of introducing a more significant waterplane stiffness was explored and found to give a pretty fair result. This is largely due to the relatively low influence of the waterplane stiffness. The motivation for introducing this is the wish to mimic more realistic conditions when fixing the structure since more of the rolling moment will move toward torsion than for the dynamic case.

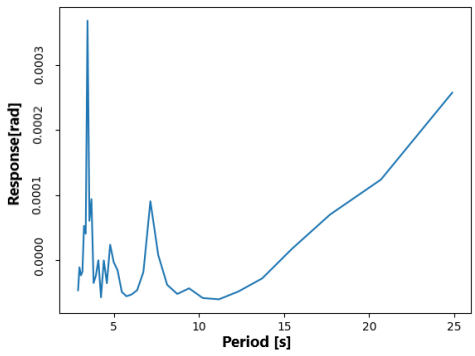

(a) No added stiffness, 0.1m waves

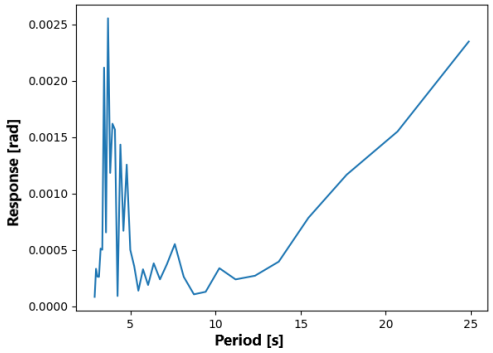

(b) No added stiffness, 1m waves

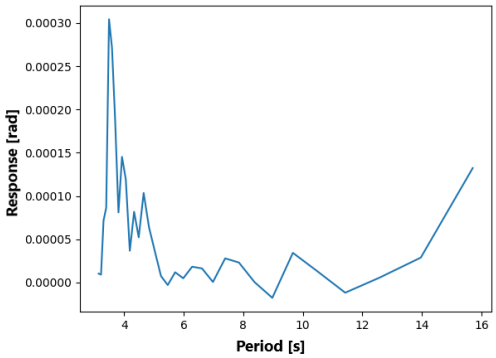

(c) Added waterplane stiffness k_{wp}, 0.1m waves

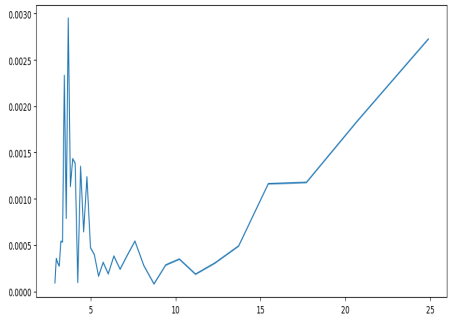

(d) Added waterplane stiffness k_{wp}, 1m waves

Figure 18: Relative roll response aft-bow, Static, with and without added waterplane stiffness

Observing that the maximum amplitude is larger for the static run, including the additional waterplane stiffness. Further yielding two high peaks with water plane stiffness and otherwise keeping large parts of the response below 0.0015 in the runs with water plane stiffness. The fact that simulations with both 1 and 2 times the water level stiffness yields the same results seem reasonable, as the water level stiffness is likely much less than the torsional stiffness in the construction. The drawback of this implementation is the reduction of the secondary eigenmode peak at 7.5 seconds, being quite clear in this static case.

3.4.2 Acceleration for different wave heights

The accuracy of the force model came to question when observing that the transfer functions developed differently for more considerable wave heights.

The wave particle acceleration is given by:

$$a = \omega^2 \xi_a \tag{32}$$

This led to examining the acceleration experienced by the structure for different wave heights. The acceleration/H for every wave height was subsequently plotted for wave heights 1-12 meters, with a constant period of 4 seconds, resulting in Figure 19.

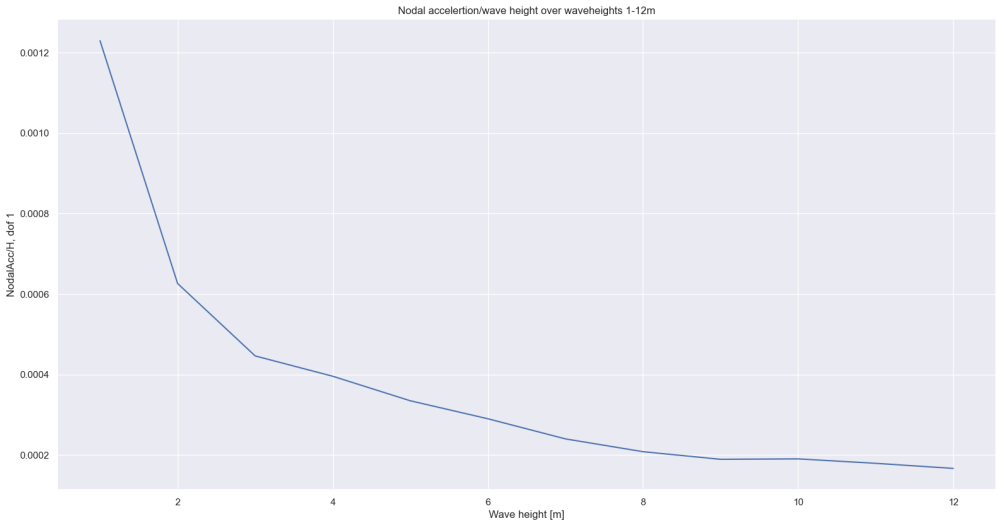

Figure 19: Acceleration/H plotted for H 1-12

Unit acceleration (acceleration divided by wave height) experienced from the structure seems to depend inversely on the wave height. This is a huge surprise, as the relationship should be constant, per Equation 32. This seems to verify the already established steepness limit, as a period of 4 seconds put into Equation 6 yields a max height for a wave to $H = 3.52[m]$. More surprising is that the relationship seems to move toward constant for the higher wave heights again. Counter intuitive this indicates that applying the largest waves again is applicable, and it is around the steepness limit itself that the most prominent issues prevail.

3.4.3 Location of fixed node

During discussions regarding what node and/or element to implement as fixed in the static analysis, the effect of the global rolling moment was discussed. Due to the starboard aft bottom node being the initial fixed node, as per Figure 15, the roll moment of the entire structure contributed to the relative role of the nodes.

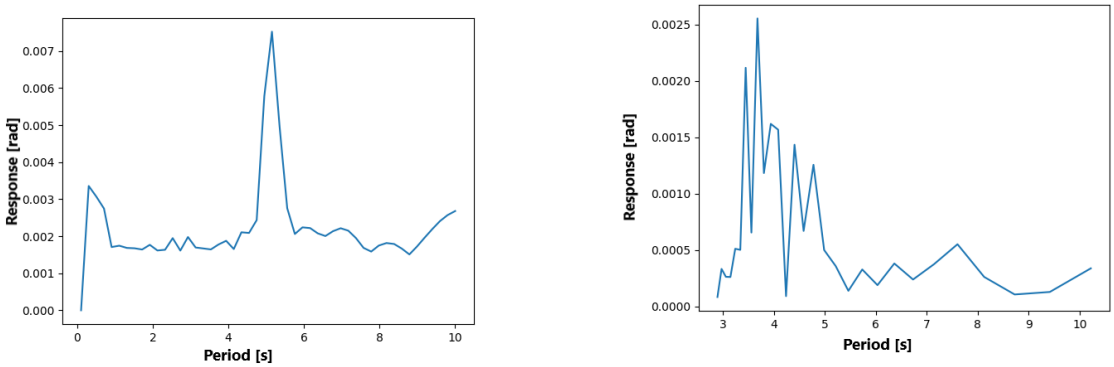

(a) Torsional response, fixed aft node, 1m waves

(b) Torsional response, fixed middle node, 1m waves

Figure 20: Comparison of relative responses in roll

As evident through comparing Figure 20a and Figure 20b reduced the recorded roll angle, by 2-5 times throughout the simulation. Another observation ot be made is the shift of the period region of the resonance peak. If the configurations are considered a clamped-free beam, this makes sense, as the geometric stiffness of the corner node will be substantially lower than for the middle fixed node.

3.4.4 Nodal choice for response retrieval

During a discussion of the results, it was pointed out that significant deviance during short ω steps might originate from the rotational nature of the nodes during more localized frame deformation, as shown in Figure 21. Further discussion was whether this bending mode might yield a non-conservative result, as the nodal rotation in Node 1 and 2 are opposite directions, leading to underestimating the response amplitude.

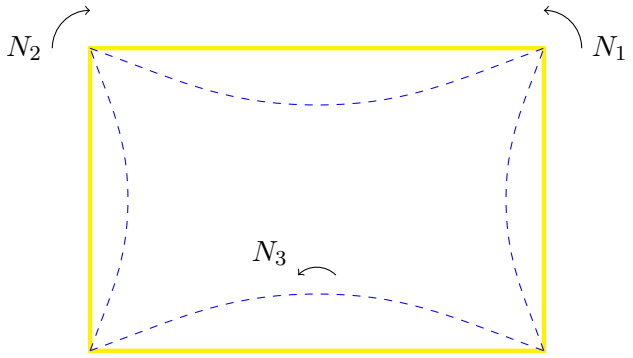

Figure 21: Nodal positions and rotation during frame bending, aft POV

To investigate the importance of this mode, the relative roll response was retrieved from both the originally suggested analysis nodes and the centerline bottom node. The plot of both these responses can be seen in Figure 22.

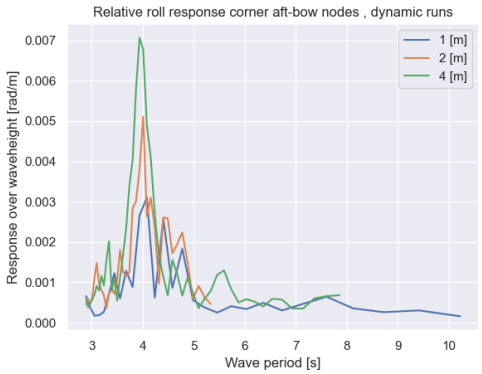

(a) Relative roll Node 1 aft to Node 2 bow

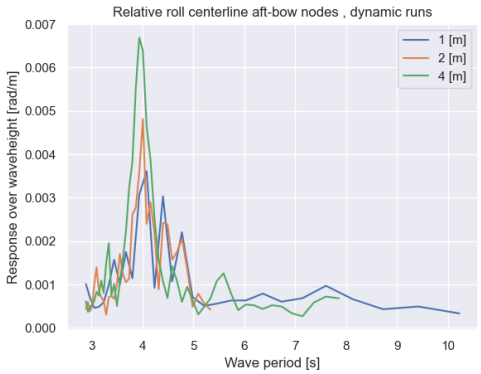

(b) Relative roll Node 3 aft to bow

Figure 22: Comparison of torsion Transfer Function foundation dependant of node examined

Through Figure 22 it becomes clear that the effect of the localized beam bending on the rotations is relatively tiny. Further, it can be seen that the corner nodes yield a more considerable response amplification, and thus the choice of corner nodes does not reduce how conservative the results become.

3.5 Resulting transfer functions

3.5.1 Torsion eigenmode

Smoothed transfer function for hull torsion, including data points.

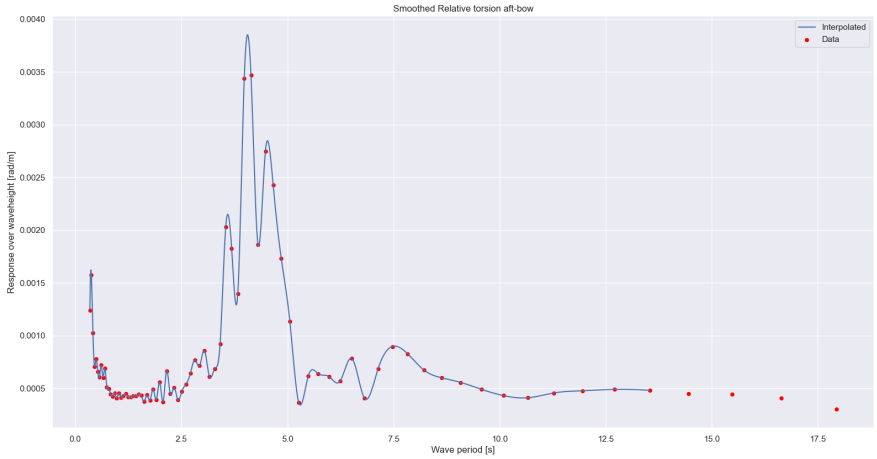

Figure 23: Transfer function for torsion

3.5.2 Vertical bending mode

Smoothed transfer function for vertical hull bending, including data points.

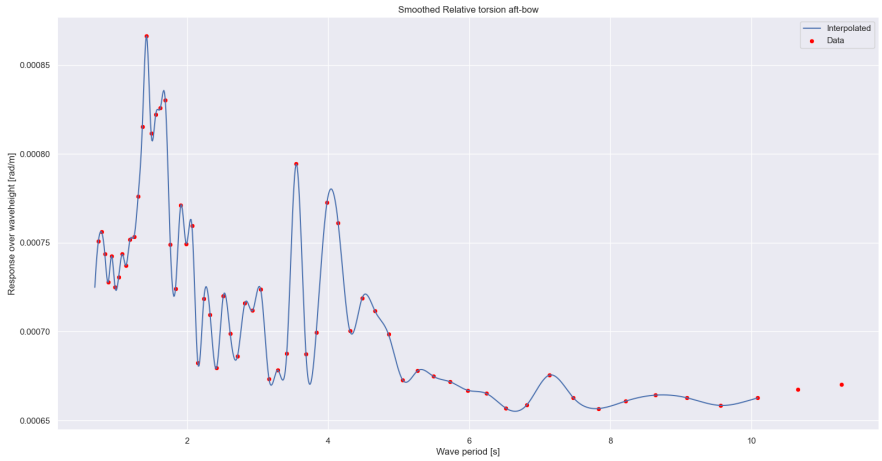

Figure 24: Transfer function for bending

Observe the three distinct peaks in Figure 23. These are hard to explain all by themselves. However, in Figure 24 observed response peaks for vertical bending of the structure lie extremely close to that of the peaks from the torsional response.

3.6 Establishment of response spectrum

Transfer functions, $R(T)$, have been established through stochastic linear simulations. A response spectrum can be calculated with $R(T)$ by combining them with a wave spectrum. In determining a wave spectrum, a critical sea state derived from the contour plot in Figure 9 is to be represented by its energy densities for the same frequencies that the transfer functions are based upon. This is then to be multiplied with the $r(s)$ squared to yield the response spectrum as given below:

$$R(T) = H(T)^2 \cdot S(f) \tag{33}$$

Where S(f) is a given storm's wave spectrum, where a practical wave analysis uses the frequency f instead of $\omega = 2\pi f$.

For this calculation, a critical sea state is to be represented through the JONSWAP spectrum. This representation is done through scripting. Utilizing the *Oeanwaves* python package, one can access the jonswap function with frequencies, significant wave height, and peak spectral period T_p as inputs. The function yields the energy densities for the given frequencies. The resulting energies over frequencies now represent the wave spectrum and are multiplied with the transfer function squared for the same frequencies.

The critical sea state has been located by evaluating the peaks in the simulated transfer function. For each sea state evaluated, stochastic simulations of said candidates have been run and located the sea state with the most significant response. This way, the sea state that is to be the created response spectrum is identified.

3.6.1 Resulting response spectrums

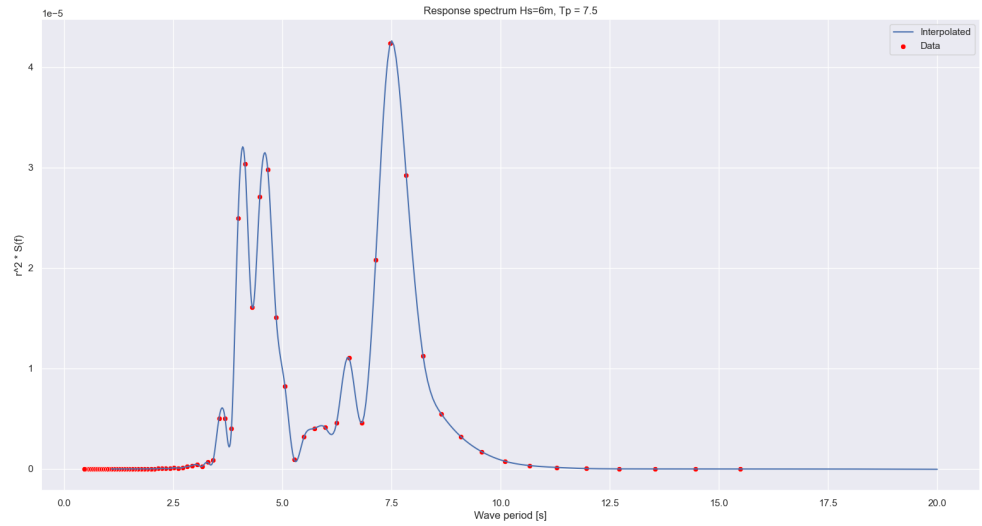

Figure 25: Response spectrum torsion, as combination of the linearly simulated transfer function and JONSWAP wave spectra($H_s = 6m$, $T_p = 7.5s$)

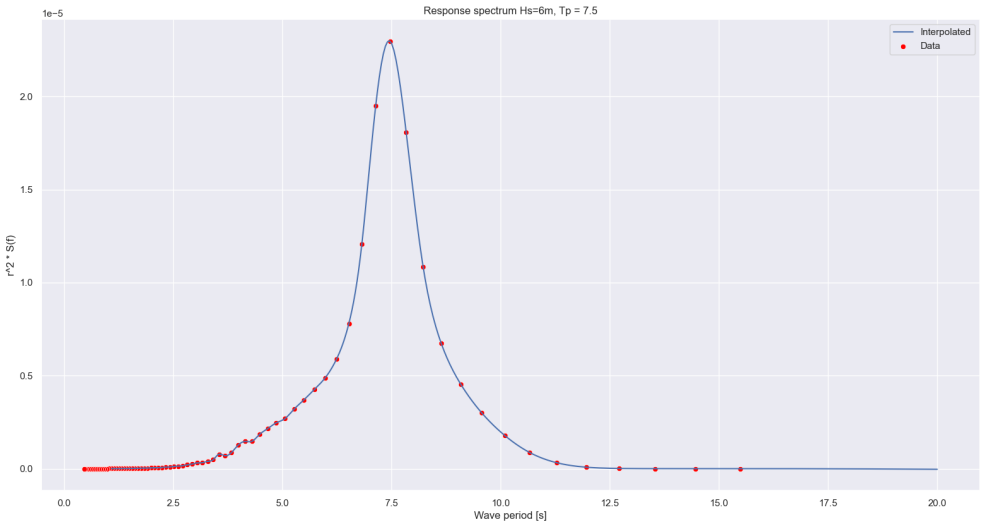

Figure 26: Response spectrum Bending, linearly simulated transfer function and Jonswap($H_s = 6m$, $T_p = 7.5s$)

3.7 Discussion

The wave steepness is a reoccurring theme in establishing transfer functions for realistic wave heights, as it yields an upper limit to the wave heights. During the examination of acceleration for different wave heights, this was evident in that the expected constant relation between acceleration/H and wave height became inverse. The fact that this relation trends toward constant for larger wave height indicated that this is a boundary value-specific problem.

Observe Figure 20a and Figure 20b and consider the difference in relative roll response. This can be explained intuitively, as the waves approach at a 45-degree angle. Thus the entire global rolling moment will contribute to the relative roll between this node and the one in the bow. Another effect will be that the relative roll aft to bow in this configuration is approximately the same as retrieving the absolute roll of the bow node, explaining the bottom line of the 2x response. Both of these factors are, of course not present in the dynamic runs (Figure 16) as the entire structure is free to rotate.

During the torsional transfer function examination, the three distinct peaks around 4 seconds were spotted. These peaks caused confusion at first. However, when comparing them to the vertical bending transfer function, it seems that these modes heavily interact. This makes sense, as any damping on the structural rotation in the aft and bow could excite the bending natural period in a manner that bends the structure.

For the static case a decreased response amplitude emerges. Further one can observe consistent but slightly lower peak response period. Both can to some degree be explained directly by the spring implementation, as some force will go to ground through this element. Static results seem to conform more to the linear responses in the same degree as dynamic case when exposed to increasing wave heights.

The wave steepness is a reoccurring theme in the establishment of transfer functions for realistic wave heights, as it yields an upper limit to the wave heights. During the examination of acceleration for different wave heights, this was evident in that the expected constant relation between acceleration/H and wave height became inverse. The fact that this relation trends toward constant for larger wave height indicate that this is a problem specific to the boundary region.

In general the results seem to be of adequate nature, and progress linearly even for more realistic wave heights.

4 Global response

The step-by-step procedure for establishing the short term extreme response value is: [12]

- Establish q-probability contour of metocean charecteristics
- Identify worst sea state (in regard to problem under consideration
- Establish distribution function of 3-hour maximum for identified sea state by time domain simulations
- Fit A Gumbel distribution to observed 3-hour extremes
- The 90-percentile then represents a good estimate for the long term value (given $q = 10^{-2}$)

For exceedance probability of high thresholds there are three variables involved; H_S, T_p and the three hour maximum value $X_{\Gamma,3h}\left(H_s, T_p\right)$. The contour line method requires many simulations to analyze the global response in irregular seas.

The long term exceedance probability for a response threshold in a 3-hour sea state is given by: [15]

$$p_f\left(x_{\Gamma,crit}\right) = \iiint_{g(\ldots)<0} f_{X_{\Gamma_{3h}}|H_sT_p}(x \mid h,t) f_{H_sT_p}(h,t) dx dt dh \tag{34}$$

This methodology can be solved through the Inverse FORM method.[41] Done through identifying the requested q-probability of the return sea state. Then, from this sea state, finding the failure/response probability as the 90th percentile of a fitted distribution for the extreme values simulated. The advantage of this is that a time-domain study allows for the usage of simulations examining the response rather than iterative prediction based on Gaussian statistics in combination with identifying the slowly varying metocean parameters involved.

4.1 Identifying worst sea state

For the q-probability contour, Figure 9 will be utilized. Some unfavourable sea state characteristics are known the transfer function established in Section 3.After examining the contour, an assortment of sea states have been simulated and compared to each other for their maximum torsional response. The maximum value sea states along the top of the contour yield the highest energy sea states. This is quite obvious as these sea states contain the largest spectrum energies. The torsional response depends strongly on the wave period, and thus the critical sea states are, for this reason, expected to be found in the lower T_p region.

4.2 Estimation of characteristic extreme response

For time-domain simulations, the short-term extreme response, Resp(max), may be extracted directly from the response time series for the critical sea state with a 100-year return period.[12] Here, Resp(max) will correspond to the 90 percentile response value from a distribution fitted to the 30 simulations run.

The recommended distribution is Gumbel for this type of problem. The simulated extreme responses were applied through a Python library with distribution functions for the distribution fitting. Resulting distribution probability plots were then evaluated visually and numerically. The distribution chosen after this is the 3-parameter Weibull distribution, shown in Figure 27. All distribution fittings can be seen in Appendix B

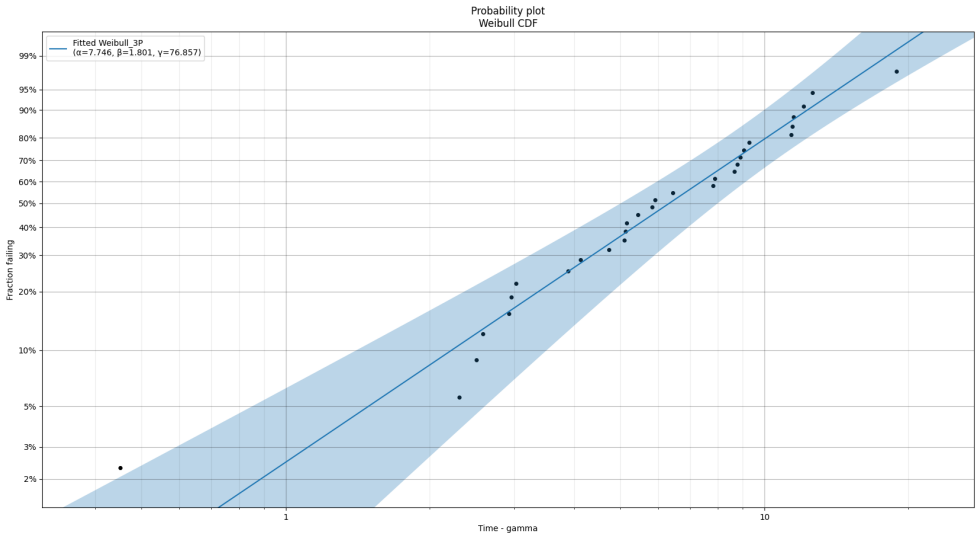

Figure 27: Fitted Weibull 3-parameter $H_s = 6[m], T_p = 7.5[s]$, responses multiplied by 10^4

In Figure 27, the weibull parameters included in Equation 12 are; $\alpha = 7.74604$, $\beta = 1.80144$ and $\gamma = 76.857$.

The 90 percentile exceedance probability for the simulated runs yields a $8.91639 * 10^{-3}[rad]$ torsional deformation of the structure. This is close to double what the unit wave transfer function, Figure 23, yields for a 1-meter wave height at resonance. This comparatively low response sparked the interest of another simulation with a lower period, to adequately examine the absolute characteristic extreme response maxima. However, it should be noted that the response still corresponds to a 30% higher response than the unit load transfer function yields for the same period as the peak sea state period, 7.5 seconds.

For this lower period critical sea state, the maximum H_s corresponding to the period yielding maximum response in the transfer function is located at the 100-year return contour line. Reading from Figure 9, the largest unit response happens at $T_p = 4.06[s] \approx 4[s]$, yielding a $H_s = 3.9[m]$ at the 100 year return contour line. Due to the relatively low variability seen in the previous 30 simulations, and time constraints regarding the analysis, the number of simulations to be run is now changed to 20, the lower statistical reliability threshold for the method. The resulting extreme responses was also fitted quite well to the Weibull 3-parameter distribution, seen in Figure 28.

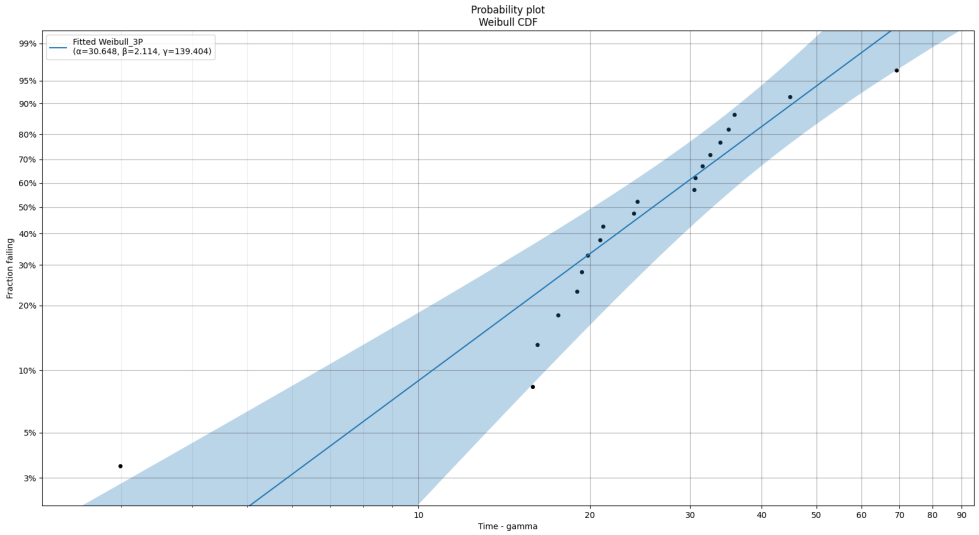

Figure 28: Fitted Weibull 3-parameter $H_s = 3.9[m], T_p = 4.06[s]$, response x 10^4

With Weibull parameters: $\alpha = 30.6483$, $\beta = 2.11423$ and $\gamma = 139.404$.

The 90 percentile for the simulated runs turns out to be $1.84874 * 10^{-2}[rad]$ torsional deformation of the structure. Evidently larger than the response from the previously examined sea state. As it is a 25% larger response than what the unit wave transfer function at resonance yields, it also is in line with the characteristic extreme response prediction from the $T_p = 7.5$ sea state. These results makes the case for confidently stating that the worst sea state with the same q-probability of return is identified to be at resonance in regard to torsion.

4.3 Discussion

For the first data set, the Gumbel distribution initially seemed like a better fit. However, the finding of a surprisingly low response value led to another set of stochastic simulations for a sea state with period close to torsional resonance. This new data set fitted better to a Weibull 3-parameter, and the initial data set was evaluated to fit adequately as well. The 7.5 second period simulations yielded a characteristic extreme response well under what could be considered extreme. This is not the case for the resonance sea state, as it nearly doubled the previous response. This backs up the claim that the most unfavourable sea state for a given q-probability of return lies in the T_p region close to resonance period. By further inspecting the contour line plot developed by MultiConsult, Figure 9, one can see that this should not be a huge concern, as the H_s in this region is extremely low. However, to confidently approve a design such as this, further FLS analysis should be carried out.

5 Analysis of net model

The net model in question was obtained through earlier master thesis written by Holen (2017) and Gulpinar (2021). Also this model had to be adjusted as described in Section 2. The model is extremely computationally demanding, and the simulations are thus reduced significantly. The original plan was to establish the methodology for the entire thesis and then simulate the same cases for the net model. However, this has proved unfeasible due to time constraints, and the only simulated case is the transfer function establishment. For the model including the net structure, it was impossible to run a flat spectrum as the analysis seemed to abort almost immediately.

5.1 Transfer function

Similar simulations were utilized to evaluate the net model to establish a torsional transfer function.

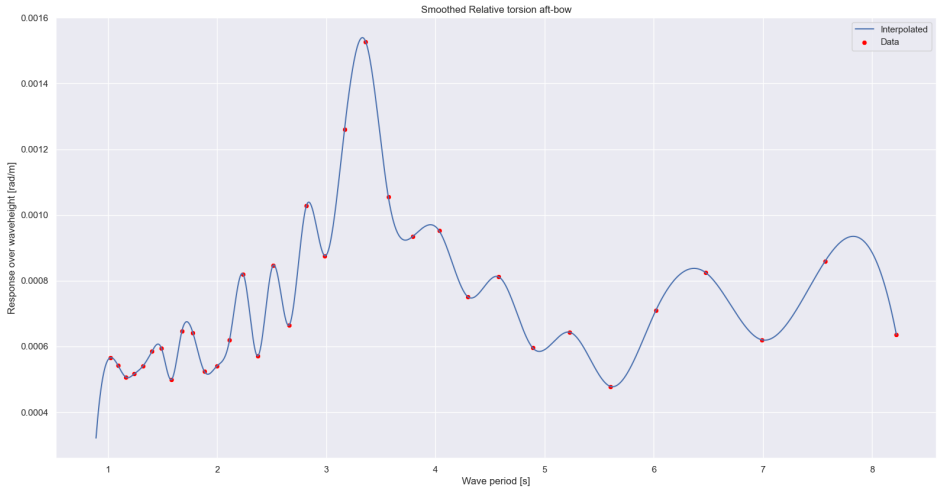

Figure 29: Torsional transfer function for the net model, flat spectrum is not subtracted.

As evident from the data points, less simulations were run for this case. This is due to the model being extremely computationally demanding and putting a large time constraint on its study.

5.2 Discussion

As can be seen from comparing Figure 29 and Figure 23, both the amplitude of unit response as well as the period of maximum response has been reduced. The decreased period peak can be explained by the modelling of the nets. Holen noted that the implementation of the nets introduced additional stiffness to the model, as such an eigenperiod reduction is as expected. [16]

6 Design wave method

The linear methods seemed to give decent results, for the most part, the exception being the linear dynamic 6m case. This indicates that the response is linearly dependent on the excitation. Thus the design wave approach shall be implemented and evaluated.

Most environmental loads of significance for column-stabilized units are those induced by waves. To establish a characteristic response, these conditions need to be described. This can either be done through stochastic methods such as the simulations performed in [**sec:trans**]. Another approach is to establish a deterministic design wave.[35] In this section, the latter option is to be explored and compared to results from the stochastic approach.

According to DNV-RP-C103, the design wave analysis can be broken into 7 steps, of which the five first are relevant for this thesis scope, as it is the maximum response itself that is aimed for, not the time dependant load effect.

- Chosing characteristic response parameters, in this case the torsional response itself
- Calculate the maximum response parameters' (Resp(max)) 90th percentile through stochastic short term analysis
- Evaluate the wavelength λ_d from the transfer function of the respective response parameter
- Calculate the wave amplitude $a_d = H/2$ through Equation 35
- Design waves are input into the global structural model and response is calculated

$$a_d = \frac{Resp(max)}{TR} \tag{35}$$

TR = Response (unit wave amplitude) for relevant wavelength

When evaluating a response through the design wave approach, the response to be evaluated needs to be carefully considered. This is done by developing a transfer function and response spectrum, yielding a tool for examining the structure's potentially unfavorable environmental conditions. [39] [35]

For increased accuracy, a range of wave periods should be investigated. However, the RP also states *"The wavelengths are selected which are the most critical to the structure or structure part to be investigated"*. This means that the periods to be investigated can be reduced to the periods already determined to yield significant responses.

The torsional response prediction should have its maxima at oblique waves placing either the entire, half, or one-fourth of the structure in either a wave trough or crest. From earlier investigations into the response spectrum, it is known that a wave period yielding large structural responses is 7.5 seconds. Additionally, creating a good baseline for comparing the two methods at hand.

From experience acquired in Section 4 this approach has its caveats and has already led to blundering by mainly examining the structure based on the developed response spectrum. As such, both the response spectrum peak at $T_p = 7.5[s]$ and the transfer function peak at $T_p = 4.06[s]$ is to be used as a basis for their respective design waves.

Another factor to consider before implementing the design wave through airy waves simulation is the wave steepness. For which the foundations are briefly explained in Section 1.5. This will provide an upper limit to check against for any design wave and corresponding period developed. If a calculated design wave case exceeds the steepness limit, the maximal steep wave will be utilized, providing the lowest possible period for the wave. The reasoning for this is the low natural periods and their considerable influence on the structural response.

6.1 Simplified design wave analysis

Similarly, one can apply a simplified design wave. This method also calls for determining the wavelength based upon experience from the stochastic analysis. However,, the wave amplitude may be determined differently bying the maximum 100-year wave steepness for regular waves. A second alternative is calculating it based on meaningful experience with the design wave approach, which this thesis' author does not consider possess, yet.

Finding the maximum steepness of the unfavourable condition $T = 7.5[s]$ found in Figure 25 into Equation 6 yields a wave height of $H = 12.49[m]$. MultiConsult calculated the individual wave height maxima with a return period of 100 years to be 11.8 meters, so this design wave can be considered conservative compared to expected conditions. [3] Calculating the max steepness wave for the transfer function maxima of $T = 4.06[S]$ in the same manner yields $H_{100RPmax,T=4.06} = 3.63[m]$.

6.2 Maximum torsion response estimated through design wave methods

In Table 4, the calculated design wave parameters for different methodologies are presented, along with their respective maximum torsional responses from simulations.

Table 4: Design wave parameters and results

Method	Tp [s]	Resp(max) [rad]	TR[$\frac{rad}{m}$]	H [m]	T[s]	Max response [rad]
Resp(max)	4,06	0,01849	0,00382	4,84	-	0,02581
Simplified	4,06	-	-	3,63	-	0,02106
Simplified	7,50	-	-	12,49	-	0,01104
Resp(max)	7,50	0,00891	0,00090	9,88	-	0,00722
MutliConsult max	-			11,8	10,1	0,00552

6.3 Maximum bending response estimated through simplified design wave method

Exploration of the bending mode was not done through the design wave method. This is due to the fact that a design wave based on the unfavourable wave periods would make for a extremely low wave, rough estimates give 0.5 meters. This is quite low, and will not provide more response than the bending transfer function itself, as it incorporates wave heights in this amplitude region.

6.4 Applicability evaluation

The simplified design wave method seems to predict the maximum response most in line with the stochastic simulations from Section 4. Further both design waves with a period at torsional resonance provide conservative results compared to previous methods. For future reference the simplified method is a strong contender for analysis as it lives up to its name. It is simple to implement and yields a quite satisfactory result. This allows an analyst to effectively predict extreme values, and thus discover problematic responses to be further investigated.

7 Conclusion -Havfarm concept evaluation

The literature review regarding relevant rules and the master thesis acquired a relevant understanding of the concept. Here the two most applicable standards are compared, The NS9415 and DNVs Rules for Offshore fish farming units. DNV rules were chosen based on their transparent reference system between documents and clear methodologies proposed for problems to be investigated. Further, the newly revised NS9415 document refers quite a bit to the DNV documents.

The model was adequately adjusted to resemble the real Havfarm 1 better. Resulting in improved estimations on the natural periods, although the roll calculation missed quite severely compared to its simulated counterparts. Some missed by up to 30%, especially problematic regarding roll. The simplified calculation in Section 2.3.4 ultimately finds potential peak periods for the torsional moment. However, it will not yield the eigenperiod for arbitrary structures. The main finding of the section being the torsional and bending eigenperiods, at 4 and 1.5 seconds.

Natural periods previously estimated, showed up again in the transfer functions established, as expected. The responses seem to follow the linear relation to the loading experienced, with the 6m dynamic case being the exception. This case seems to be a problem introduced by the exceeded wave steepness limit.

Results indicate that linear methods are a reasonable basis for evaluating the responses. Although there is conformity to be seen, some care must be taken regarding the wave steepness limit when establishing transfer functions.

Adequate correspondence to the relative responses found through the linear method used in Section 3. Considering the characteristic extreme response levels found through stochastic simulations of sea states based on the contour line method in Section 4. The Resp(max) was found to be $1.84874 * 10^{-}2[rad]$ relative roll, aft to bow

As expected, the inclusion of the net shifts the natural period slightly lower, and its amplitudes are severely decreased. The expectation is based on the introduced additional stiffness commented by Holen in his master thesis.[16] Due to time constraints, no critical sea state evaluations have been made with the net model.

Regarding design wave methods, they seem applicable. However, most of them, excluding the simplified design wave approach, identify critical environmental conditions based on the contour plots combined with the transfer functions. They may become equally tedious or computationally demanding when they are based on more "shooting in the dark" and then extracting the critical responses in the aftermath. The simplified method is a robust analytical tool and has the benefit of being relatively simple to implement. Further, the results seem to conform well to all other methods identified for the Havfarm concept.

Havfarm is quite a unique structure. Thus the level of similarity between the methods is surprising to some degree. However, the results further motivate the usage of several methods in a combination. Furthermore, comparing with actual measurements from the structures modeled will be essential for tuning these methods to precisely predict responses in innovative structures to be developed in the future.

7.1 Recommended further work

What follows are some recommendations and suggestions for further work to look into. Forming a suggested continuation of the thesis scope for further studies, and may be taken as a list of what could have improved the accuracy/reliability of the results achieved in this thesis.

Adjusting model for FLS

As mentioned in Section 2, the joint implementation is not suitable for a FLS analysis. Recommended further model improvement is thus to more accurately describe the structural members intersection making high quality local stress calculations and fatigue estimations viable.

Filtering coupled responses

To better analyze the simulated natural periods, the responses should be filtered so that the heave response is not influential in the measurements. The model has been refined to a large degree, but the coupling is of course still present, especially in regard to the pitch decay test.

Complete all static analyses with the same fixed nodes

While performing the 10 meter wave height analysis, USFOS was struggling to complete the simulations as the rotation at the control nodes were excessive. After reviewing the implementation of the fixed node, it was determined to half its stiffness and apply it to the two nodes below the columns at the middle. As these connection are significantly stronger than the beam running along the middle the rotations should not be troubling for the analysis. This model change alters the global resistance and could introduce uncertainty of the foundation for comparing the results. This should be investigated, would recommend running all static analyses with this condition. Another method to achieve compliance during the simulations would be to increase the yield strength of the relative weak transverse member which contains the fixed node.

Catenary mooring

There was attached a mooring force to the bow and the to balance out this force it was introduced an unrealistically large buoyancy element to the bow section. This has since been removed, and the spring has been modified as to not produce such a large vertical force. However, this is hardly realistic itself and thus the modelling of a catenary-based mooring system is of interest. A starting point for this could be Appendix C in Holen 2017, where he describes approach that ultimately was abandoned due to time constraints. [16]

Extend the data foundation for larger statistical power

For the establishment of statistical distribution of the critical sea state examined from the contour plot there has only been used 30 seeds, this to meet the lower threshold of a statistical study. This was implemented due to time constraints and computational demand. This number of simulations should be massively increased for increased statistical power.

Further investigation into the 6-metre dynamic case

For this case it initially seems to be dependant on the wave steepness. This is however not the case for dynamic 10-meter wave loading, nor for static 6 and 10-meter cases. Investigate the model acceleration for wave heights as attempted in Section 3.4.2.

Bibliography

[1] ABL-group. *Single Voyage Transport Tow Approval – 2020*. 2020. URL: https://abl-group.com/case-studies/havfarm-1-jostein-albert-single-voyage-transport-tow-approval-2020/.

[2] Jørgen Amdahl et al. 'TMR4105-Marin teknikk grunnlag'. In: *Akademika* (2014).

[3] NORDLAKS OPPDRETT AS. *Sluttrapport Prosjekt Havfarm 1*. 2021. URL: https://www.nordlaks.no/utvikling/havfarm1.

[4] Eric Bertin and Maxime Clusel. 'Generalized extreme value statistics and sum of correlated variables'. In: *Journal of Physics A: Mathematical and General* 39.24 (May 2006), pp. 7607–7619. DOI: 10.1088/0305-4470/39/24/001. URL: https://doi.org/10.1088/0305-4470/39/24/001.

[5] LARS BJÖRNSSON. 'Comparison of Idealized 1D and Forecast 2D Wave Spectra in Ship Response Predictions'. In: (2013). URL: https://www.diva-portal.org/smash/get/diva2:706783/FULLTEXT01.pdf.

[6] Mauro Caresta. *Vibrations of a Free-Free Beam*. 2010. URL: http://www.varg.unsw.edu.au/Assets/link%20pdfs/Beam_vibration.pdf.

[7] NSk Ship Design. *Concept evaluation presentation NSK Ship Design*. 2016. URL: https://www.sdir.no/globalassets/sjofartsdirektoratet/fartoy-og-sjofolk---dokumenter/ulykker-og-sikkerhet/sjosikkerhetskonferansen-2016-dag-1/12.-hakon-adnanes---presentasjon-havfarm-2016-09-28-sdir-design-utfordringer-eksponert-sendes.pdf?t=1582679715061.

[8] Armin Walter Doerry. *MODELLING OF HYDRODYNAMIC LOADS ON AQUACULTURE NET CAGES BY A MODIFIED MORISON MODEL*. 2008. URL: https://www.researchgate.net/figure/Illustration-of-Metacenter-and-Metacentric-Height_fig6_255202166.

[9] Odd Faltinsen. *Sea loads on ships and offshore structures*. Vol. 1. Cambridge university press, 1993.

[10] Directorate of Fisheries. *Development Licenses*. 2021. URL: https://www.fiskeridir.no/Akvakultur/Tildeling-og-tillatelser/Saertillatelser/Utviklingstillatelser.

[11] Nærings- og fiskeridepartementet. *NYTEK-forskriften*. 2011. URL: https://lovdata.no/dokument/SF/forskrift/2011-08-16-849.

[12] Zhen Gao. *TMR4195 - Design of marine structures, Lecture Notes*. 2021.

[13] Hamidreza Ghafari and Morteza Dardel. 'Parametric study of catenary mooring system on the dynamic response of the semi-submersible platform'. In: *Ocean Engineering* 153 (2018), pp. 319–332. ISSN: 0029-8018. DOI: https://doi.org/10.1016/j.oceaneng.2018.01.093. URL: https://www.sciencedirect.com/science/article/pii/S002980181830101X.

[14] Jørgen Gulpinar. 'Analysis of the Havfarm concept for extreme enviornmental loads'. MA thesis. NTNU, 2017.

[15] Sverre Haver. *METOCEAN MODELLING AND PREDICTION OF EXTREMES*. Vol. 1. Haver havet, University in Stavanger, ntnu, 2019.

[16] Vegard Holen. 'Ultimate Limit State Analysis of Havfarm'. MA thesis. NTNU, 2021.

[17] Tom Irvine. 'Bending frequencies of beams, rods, and pipes'. In: *Compare* 500.s50 (2012), pp. 31–38.

[18] Tom Irvine. *Bernoulli-Euler Beams*. URL: https://endaq.com/pages/bernoulli-euler-beams.

[19] Jan Mathisen and Elzbieta Bitner-Gregersen. 'Joint distributions for significant wave height and wave zero-up-crossing period'. In: *Applied Ocean Research* 12.2 (1990), pp. 93–103. ISSN: 0141-1187. DOI: https://doi.org/10.1016/S0141-1187(05)80033-1. URL: https://www.sciencedirect.com/science/article/pii/S0141118705800331.

[20] Emiel Mobron et al. 'Design of Havfarm 1'. In: *WCFS2020*. Ed. by Łukasz Piatek et al. Singapore: Springer Singapore, 2022, pp. 99–111. ISBN: 978-981-16-2256-4.

[21] J.R. Morison, J.W. Johnson and S.A. Schaaf. 'The Force Exerted by Surface Waves on Piles'. In: *Journal of Petroleum Technology* 2.05 (May 1950), pp. 149–154. ISSN: 0149-2136. DOI: 10.2118/950149-G. eprint: https://onepetro.org/JPT/article-pdf/2/05/149/2238818/spe-950149-g.pdf. URL: https://doi.org/10.2118/950149-G.

[22] Nordlaks. *Technical description Havfarm 1*. 2021. URL: https://www.nordlaks.no/utvikling/havfarm1.

[23] Standards Norway. *NS 9415.E:2009 Marine fish farms - Requirements for site survey, risk analyses, design, dimensioning, production, installation and operation*. 2009. URL: https://www.standard.no/no/Nettbutikk/produktkatalogen/Produktpresentasjon/?ProductID=402400.

[24] Standards Norway. *NS9415:2021 - Floating aquaculture farms; Site sruvey, design and use*. 2021. URL: https://www.standard.no/no/Nettbutikk/produktkatalogen/Produktpresentasjon/?ProductID=1367329.

[25] Department of Marine Technology NTNU. *IMT Software Wiki - LaTeX*. URL: https://www.ntnu.no/wiki/display/imtsoftware/LaTeX (visited on 15/09/2020).

[26] O.G.Houmb and T.Overvik. 'Parametrization of Wave Spectra and Long Term Joint Distribution of Wave Height and Period'. In: *First International Conference on Behaviour of Offshore Structures* (1976).

[27] Jørgen Amdahl Pål T. Bore and David Kristiansen. *MODELLING OF HYDRODYNAMIC LOADS ON AQUACULTURE NET CAGES BY A MODIFIED MORISON MODEL*. 2017.

[28] Bjørnar Pettersen. 'Marin teknikk 3 Hydrodynamikk, Pensumhefte'. In: *Norge: Akademika* (2020).

[29] *Reliability - A Python library for reliability engineering*. https://reliability.readthedocs.io/en/latest/index.html. Accessed: 2022-05-30.

[30] Copyright © 2016-2019 by Samantha James Roland Stull. *UBC ATSC 113 - Weather for Sailing, Flying Snow Sports*. 2019. URL: https://population.un.org/wpp/Graphs/Probabilistic/POP/TOT/900.

[31] Ernst Eberg Tore Holmås Tore H. Søreide Jørgen Amdahl and Øyvind Hellan. *USFOS - A Computer Program for Progressive Collapse Analysis of Steel Offshore Structures. Theory Manual*. 1988. URL: https://usfos.no/manuals/usfos/theory/documents/Usfos_Theory_Manual.pdf.

[32] Ernst Eberg Tore Holmås Tore H. Søreide Jørgen Amdahl and Øyvind Hellan. *USFOS - Hydrodynamics Theory Description of use Verification*. 2010. URL: https://usfos.no/manuals/usfos/theory/documents/Usfos_Hydrodynamics.pdf.

[33] *Simplified Double Peak Spectral Model For Ocean Waves*. Vol. All Days. International Ocean and Polar Engineering Conference. ISOPE-I-04-289. May 2004. eprint: https://onepetro.org/ISOPEIOPEC/proceedings-pdf/ISOPE04/All-ISOPE04/ISOPE-I-04-289/1852112/isope-i-04-289.pdf.

[34] Population Devision United Nations DESA. *UN world population prediction*. 2019. URL: https://population.un.org/wpp/Graphs/Probabilistic/POP/TOT/900.

[35] Det Norske Veritas. *DNV-RP-C103 Column-stabilised units*. 2015.

[36] Det Norske Veritas. *DNV-RP-C203 - Fatigue design of offshore steel structures*. 2019.

[37] Det Norske Veritas. *DNV-RP-C205 - Environmental conditions and environmental loads*. 2019.

[38] Det Norske Veritas. *DNV-RU-OU-0503 - Offshore fish farming units and installations*. 2021.

[39] Det Norske Veritas. *DNV-RU-SHIP Pt.3 Ch.4 Loads*. 2021.

[40] Det Norske Veritas. *DNVGL-CG-0130 Wave loads*. 2021.

[41] Steven R Winterstein et al. 'Environmental parameters for extreme response: Inverse FORM with omission factors'. In: *Proc. 6th Int. Conf. on Structural Safety and Reliability, Innsbruck, Austria*. 1993.

Appendix

For the input files for USFOS, see separate files attached.

A Literally hand calculations

Heave Natural Period

$$T_{n3} = 2\pi\sqrt{\frac{M + A_{33}}{\rho g A_w}} \qquad * A_{33} \in [0.6, 1]$$

$\Rightarrow$ m from ustos: $\frac{\bar{T}_B}{g} = m = 3.313 \cdot 10^7 \text{ kg}$

$A_{wp} \simeq 420 m^2$

$$T_{n3} = 2\pi\sqrt{\frac{3.313 \cdot 10^7 (1 + A_{33})}{420 m^2 \cdot 9.81 \cdot 1025}} = \begin{cases} 24.9 \text{ s} & (A_{33} = M) \\ 22.3 \text{ s} & (A_{33} = 0.6M) \end{cases}$$

$t_{crest}(s) = 16, 39, 62, 86, 109, 133, 156$

$$\frac{156 - 16}{6} = 23.3 \text{ s} \Rightarrow \left(\frac{T_{n3}}{2\pi}\right)^2 = \frac{M + A_{33}}{\rho g A_{wp}}$$

$$\left(\frac{T_{n3}}{2\pi}\right)^2 \rho g A_{wp} = M + A_{33}$$

$$A_{33} = \left(\frac{T_{n3}}{2\pi}\right)^2 \rho g A_{wp} - M$$

$$= 2.510 \cdot 10^7$$

$$\Rightarrow A_{33} = 0.76M$$

Roll Natural Period

$\overline{GM_T} = KB + BM - KG$ $\qquad BM = \frac{I}{\nabla}\ [m]$

I: * Neglect Boat cylinder (low contribution)

4x small vertical columns: $(4m)^2 = 16m^2$

3x large -"- -"- $\rightarrow 40m^2$

+ small front column $\rightarrow 16m^2$

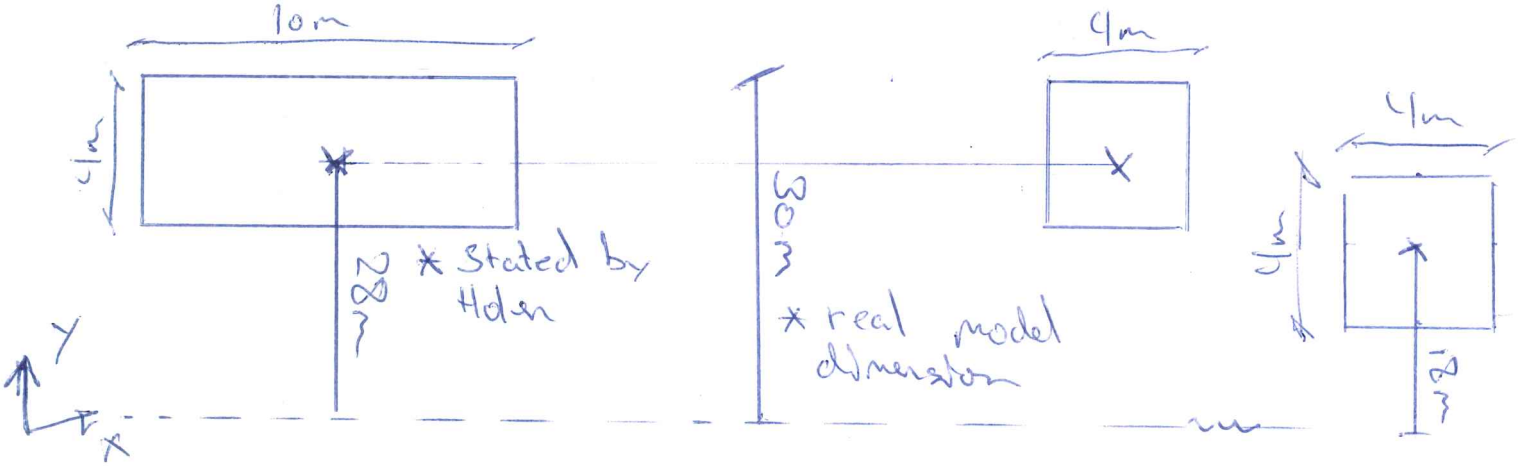

$$I = \{4 \times 16m^2 (30m)^2 + 3 \times 40m^2 (30m)^2 + 16m^2 \cdot (20m)^2\} \cdot 2$$

$$= 2\{\underbrace{57\,600m^4}_{4\ small} + \underbrace{108\,000m^4}_{3\ large} + \underbrace{6\,400m^4}_{front}\} = 344\,000m^4$$

*Compare to $I_{w=22m} \simeq 298\,880m^4$ $\qquad \Delta I\ (30 \leftrightarrow 28N) = 15\%$

$\nabla \simeq 35\,000\,000\,kg$

$$T_{n4} = 2\pi\sqrt{\frac{M \cdot r_{44}^2 + A_{44}}{M \cdot GM_T}}$$

$$\Rightarrow T = 2\pi\sqrt{\frac{r_{44}^2 + 1}{GM_T}} \quad USFOS$$

$r_{44} \simeq k = \sqrt{\frac{I}{A}} \simeq$

$*A_{44} \simeq M$ $\qquad A$ = area + "added area" $\rightarrow$ Area x 2 =

$\Rightarrow r_{44} = 20.7m$

$A_{44} \simeq 0.6 \rightarrow 23.2m$

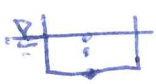

$I_{KG} = KB + GB$

$\Rightarrow GM = KB + BM - (KB + GB)$

$= BM - GB$

$$BM = \frac{344\,000\,m^4}{32321} = 10.64m$$

$KG \rightarrow USFOS \rightarrow 6m$

$BG \rightarrow USFOS \rightarrow -2.58m$

$GM = 10.64 + 2.58 = 13.22$

$$T_{n4} = 2\pi\sqrt{\frac{20.7^2 + 1}{13.22}} = 35.8s$$

($r_{44} = 23.2m \rightarrow 40.2s$)

Bending Stiffness Frequency

* Source: Tom Irvine – "Intro to shock..."

$$\omega_n = \beta_n^2 \sqrt{EI/\mathcal{J}_L}$$

$$\Rightarrow f_n = \frac{1}{2\pi}\left[\frac{22.373}{L^2}\right]\sqrt{EI/\mathcal{J}_L} \qquad (1)$$

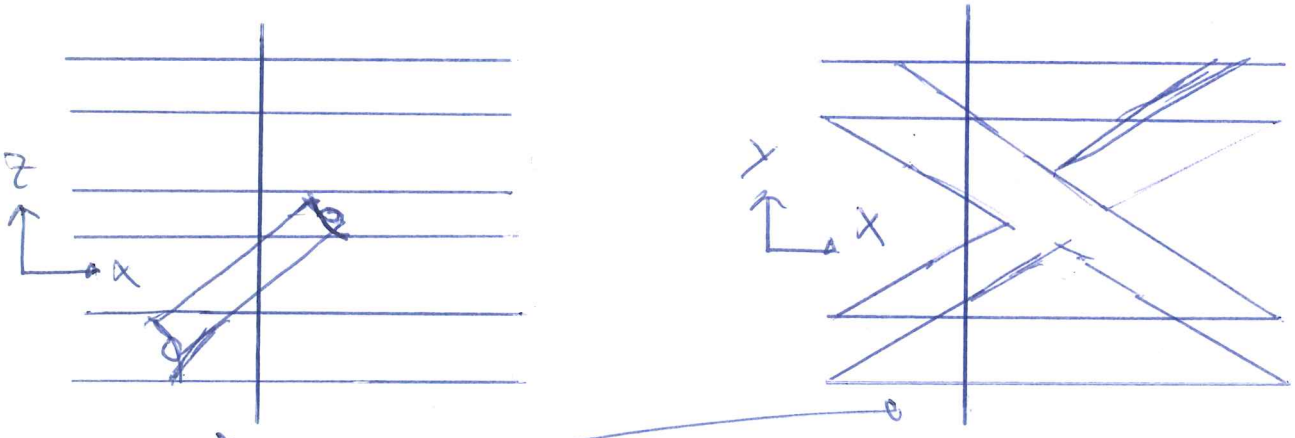

Cross-section assumed const $\Rightarrow EI(x_1) = EI(x_n)$

Center of Area (symmetry used): $\frac{\sum A_i \cdot a_i}{\sum A_i} \Rightarrow \frac{55.51\ m^3}{3.781\ m^2} = \underline{14.68\ m}$

~~I~~ = * Assume angle of braces will not reduce stiffness too much $\Rightarrow$ take area of brace cross-section

$I_y = \sum A_i \cdot (a_i)^2 \qquad a_i = (\text{"z-coordinate"} \pm_n 14.68\ m)^2$

$\Rightarrow I_y \simeq 1480\ m^4 \rightarrow EI_y = 310800\ [m^4 \cdot GPa]$

$L = (336 \leftrightarrow 396)\ m$
$m \simeq 35000000\ kg$ } $\mathcal{J}_L \simeq \frac{M}{L} = 3.11 \cdot 10^4 \frac{N}{m^2}$
$m_A \simeq m \Rightarrow M = 2m = 7 \cdot 10^7\ kg$

$$f(L=396m) = 0.95\ Hz, \quad f(L=336m) = 1.22\ Hz$$

$\underline{T_{n,L=396m} \simeq 1.05\ s}$, $\underline{T_{n,L=336m} \simeq 0.82\ s}$

Model adjustments (mass, displacement)

STO

- original mass: 31 270 353.34 kg (B)
  modified mass: 32 612 432.29 kg (A)
  diff → 1 342 078.95 kg
  % diff → +4.29 %

* Assume Draught at even keel is ~~D~~ 30m = D

original bow_pipe_disp = ~~D πr²~~ wetted height · πr² ⇒ 10m · π · 10² = 10³π = 3141.60 m³

- modified bow_pipe_disp = 30m · π · (2.5)² = 589.05 m³
  diff → −2552.54 m³
  % diff → $-\frac{13}{16}$ = −81.25 %

Additional beam elements in Bow:

Transverse beam : h · w · L = 3 · 4 · 40 m³ = 480 m³

Diagonal transversly beams (support for pipe) = 3 · 4 · 28.28 · 2 = 678.72 m³

Diagonal height pipes = 2 · 28.72 · π · $(\frac{2.5}{2})^2$ = 281.96 m³ ·x2 = 563.92 m³

- Total additional ∇ = ~~1440.68 m³~~ → 1722.64 m³

⇒ Total Δ disp = −(2552.54 − 1722.64) m³
= 829.9 m³

% diff disp = ~~26.42 %~~ ≃ 2.628 %
⇒ 2.6 %

$$\frac{829.9 \cdot 1025}{31270353 + 1100 \cdot 10^3}$$ = 0.02628

(1100 · 10³: Nodal masses)

-

B Extreme response value probability fitting

A Fitted data for Hs=6, Tp=7.5

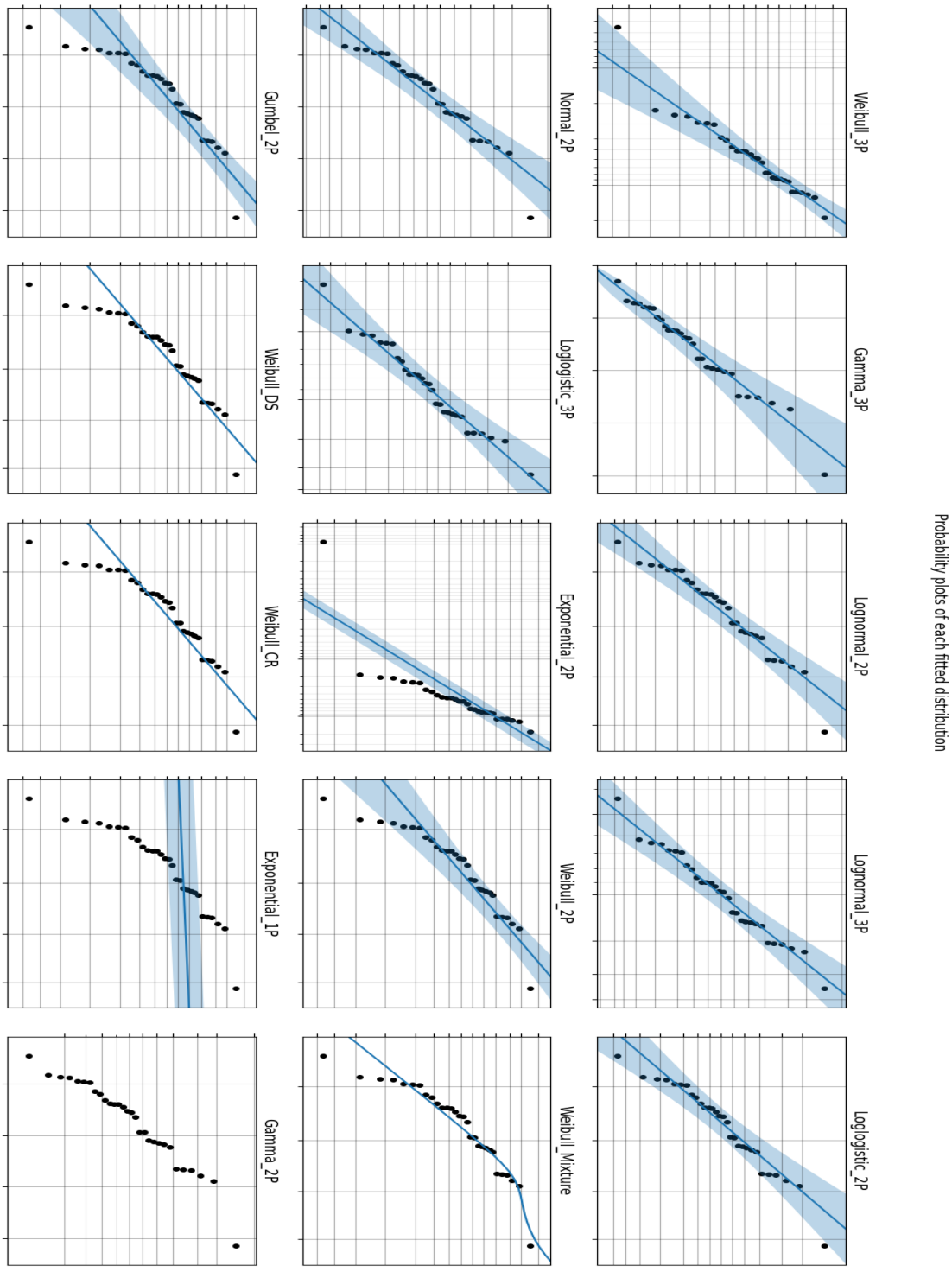

B Fitted data for Hs=6, Tp=7.5

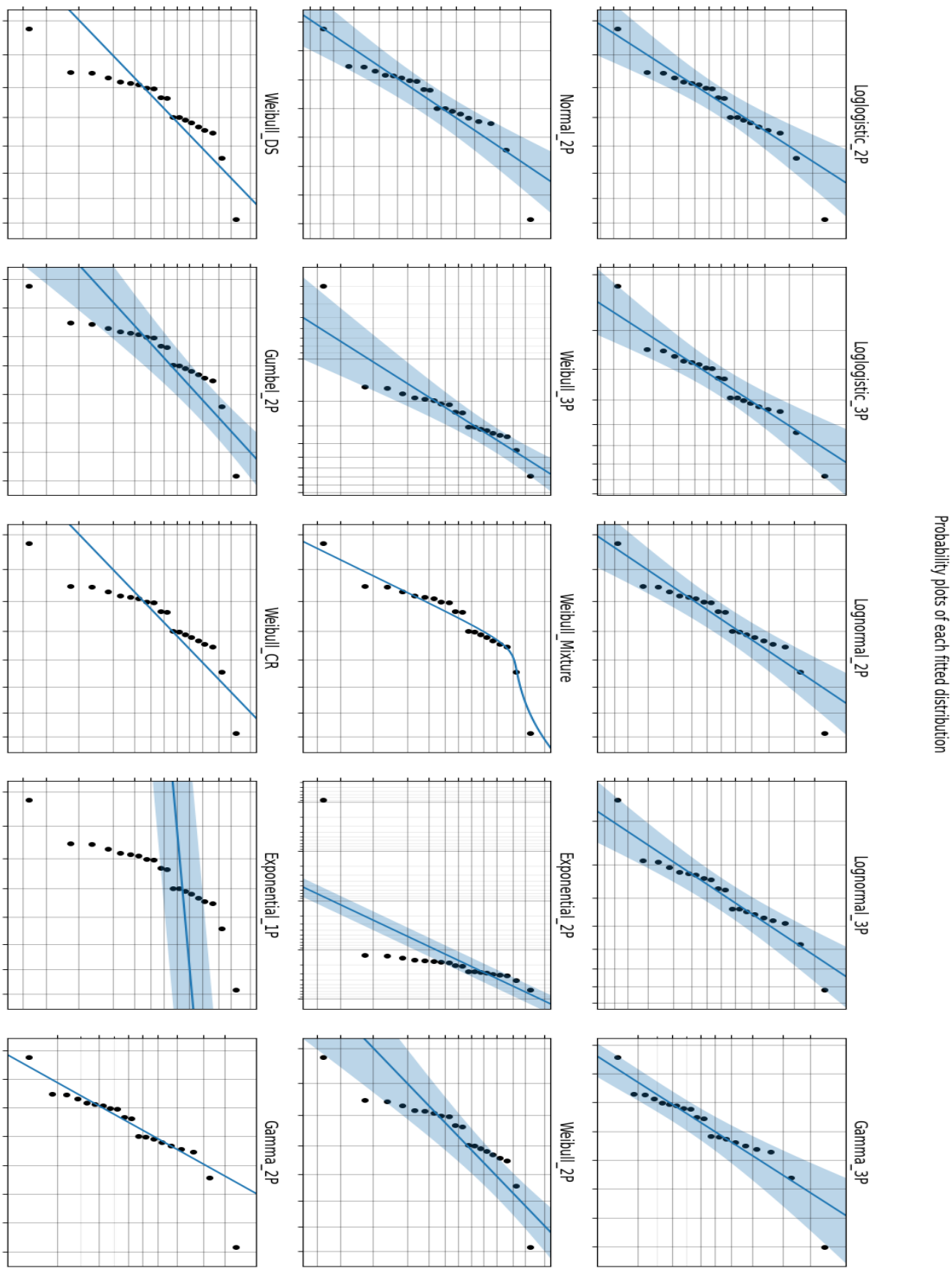

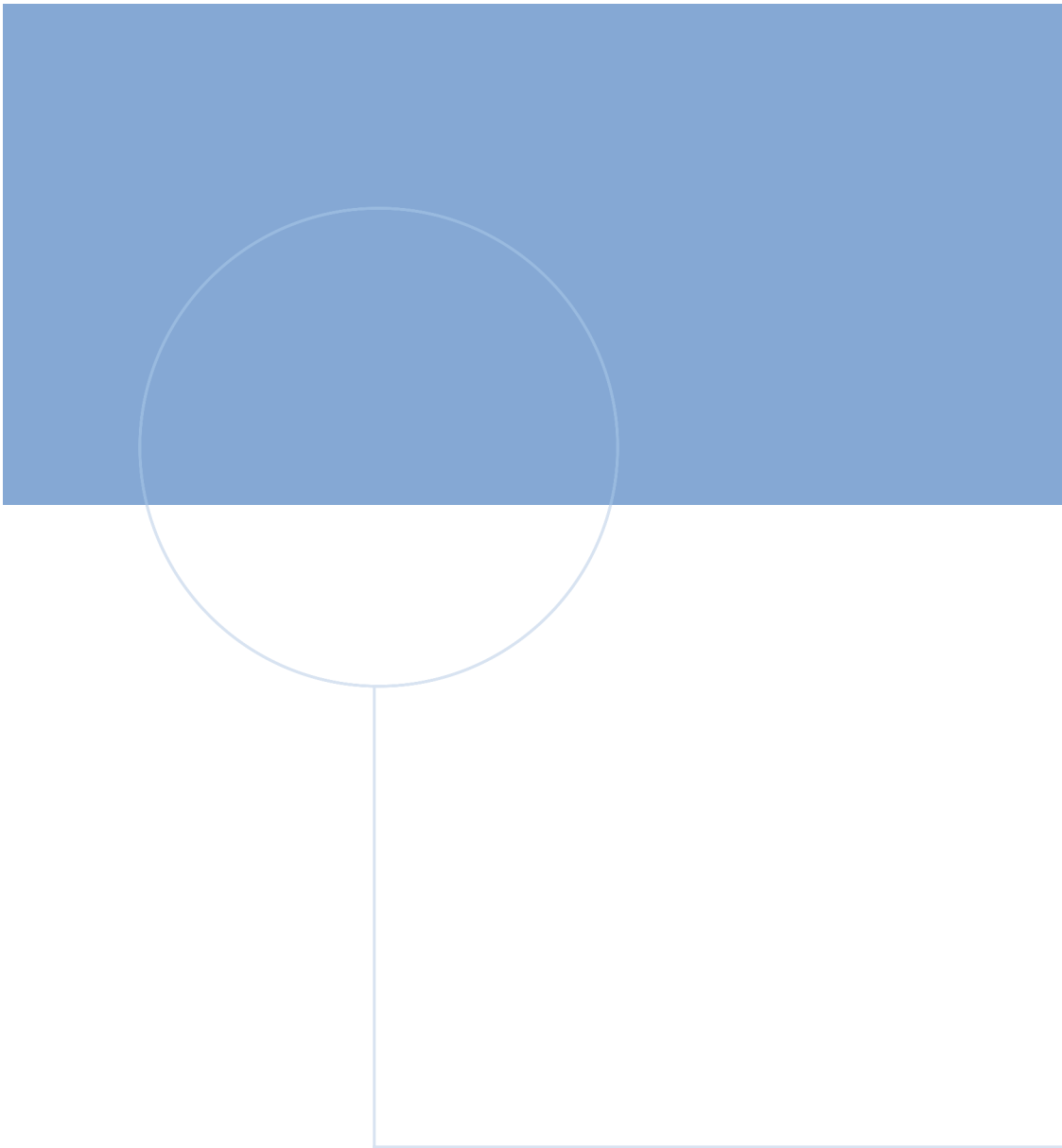

NTNU

Norwegian University of
Science and Technology